A GRID OF NON-LTE LINE-BLANKETED MODEL ATMOSPHERES OF O-TYPE STARS

Thierry Lanz[1]

Department of Astronomy, University of Maryland, College Park, MD 20742; lanz@stars.gsfc.nasa.gov

and

Ivan Hubeny[1]

National Optical Astronomy Observatory, P.O. Box 26732, 950 North Cherry Avenue, Tucson, AZ 85726;
hubeny@tlusty.gsfc.nasa.gov
Received 2002 October 7; accepted 2003 January 28

ABSTRACT

We have constructed a comprehensive grid of 680 metal line–blanketed, non-LTE, plane-parallel, hydrostatic model atmospheres for the basic parameters appropriate to O-type stars. The OSTAR2002 grid considers 12 values of effective temperatures, $27,500 \text{ K} \leq T_{\rm eff} \leq 55,000 \text{ K}$ with 2500 K steps, eight surface gravities, $3.0 \leq \log g \leq 4.75$ with 0.25 dex steps, and 10 chemical compositions, from metal-rich relative to the Sun to metal-free. The lower limit of $\log g$ for a given effective temperature is set by an approximate location of the Eddington limit. The selected chemical compositions have been chosen to cover a number of typical environments of massive stars: the Galactic center, the Magellanic Clouds, blue compact dwarf galaxies like I Zw 18, and galaxies at high redshifts. The paper contains a description of the OSTAR2002 grid and some illustrative examples and comparisons. The complete OSTAR2002 grid is available on-line.

Subject headings: methods: numerical — radiative transfer — stars: atmospheres — stars: early-type

1. INTRODUCTION

Theory of stellar atmospheres is presently enjoying a period of revival. This renewed interest has several major reasons. On the observational side, there has been an unprecedented expansion of quantity and quality of stellar spectrophotometric observations. Thanks to high sensitivity and high signal-to-noise ratio, one can now routinely record good-quality spectra of individual stars in other galaxies than the Milky Way, thus giving birth to a field of extragalactic stellar astronomy (Kudritzki 2000). The importance of deriving accurate stellar parameters as significant constraints for the global galactic and cosmological parameters, coupled with the quality of observations, compels us to use as accurate and reliable model atmospheres as possible.

Among all stellar types, the hot, massive, and bright stars, in particular O-type stars, stand as one of the most important stellar groups in the global astronomical context. They contribute most of the radiation to the UV and optical integrated spectra of galaxies that still undergo a star-forming process. The O stars provide the majority of ionizing photons for H II regions, as well as the interstellar and intergalactic medium. In the cosmological context, there is still a debate whether hot massive stars or active galactic nuclei provided the necessary photons for the reionizing of the universe around $z \approx 3$. In view of forthcoming space missions, like the *James Webb Space Telescope*, there is a growing interest in studying the early (or even the first) generation of stars in the universe (see, e.g., Weiss, Abel, & Hill 2000).

On the modeling side, the capabilities of the modeling methodology have advanced enormously. One obvious reason is a manyfold increase of computer speed and memory.

Another, and also very important, reason is the development of efficient and robust numerical methods. The central role in this respect is played by the accelerated lambda iteration (ALI) method (for a recent review see Hubeny 2003).

With the development of fast computers and efficient numerical methods, the basic limiting factor is now becoming the accuracy (and availability) of atomic data. Fortunately, great advances are being made in this direction too. Recently, two major collaborative projects, the Opacity Project (OP; Seaton 1987; Opacity Project Team 1995, 1997), its continuation the IRON Project (Hummer et al. 1993; Pradhan et al. 1996; Nahar 2003), and the OPAL project (Iglesias & Rogers 1991, 1996), have produced atomic data on a large scale.

The time is thus ripe to compute a new grid of model stellar atmospheres. We need to analyze spectra of individual stars, as well as composite spectra of galaxies, with much larger degree of complexity and accuracy than is provided by the Kurucz (1993) spectral energy distributions (SEDs) currently in use.

Because of the importance of O-type stars, such a modeling effort is hardly new. However, there are three issues that make a construction of O star model atmospheres a highly nontrivial task: (1) the presence of a strong mass outflow, the stellar wind; (2) significant departures from local thermodynamic equilibrium (LTE); and (3) an effect of numerous metal lines, traditionally called metal line blanketing. At present, there are no models that would address all three of these issues in full (that is, to construct fully blanketed, non-LTE [NLTE] models for an entire atmosphere, going from essentially static photosphere out to the wind—the so-called unified models), although there are several research groups and several computer programs that are in principle capable of doing so: CMFGEN (Hillier & Miller 1998; Hillier 2003), Hoeflich's suite of programs (Hoeflich 1995, 2003), PHOENIX (Hauschildt, Baron, &

[1] Laboratory for Astronomy and Solar Physics, NASA Goddard Space Flight Center, Code 681, Greenbelt, MD 20771.

Allard 1997), Munich programs (Pauldrach, Hoffmann, & Lennon 2001), and the Kiel-Potsdam code (Hamann 1985; Koesterke, Hamann, & Graefener 2002).

As we will discuss in more detail in the next section, either unified models require huge computer resources, or one has to approximate the other two ingredients: NLTE and line blanketing. In addition, a description of a stellar wind is still somewhat uncertain. It is therefore desirable to be able to construct complete models for hydrostatic layers, traditionally called the stellar photosphere. Even this simplified problem is a tremendous task. Early NLTE model atmospheres (Auer & Mihalas 1969b; Mihalas 1972) considered only a few (about 10) energy levels of H and He. Likewise, only the most important opacity sources were considered: several bound-free transitions of H and He and a few of the most important hydrogen lines. On the other hand, both observations and LTE line-blanketed models (Kurucz 1979) showed that the UV spectrum contains a huge number of metal (mostly iron) lines, which may then significantly influence not only the emergent SED but also the atmospheric structure in general.

Although it was clear that early NLTE models provided a significantly improved prediction of line profiles of the most important spectral lines (see, e.g., a number of papers in Garmany 1989; Crivellari, Hubeny, & Hummer 1991; Heber & Jeffery 1992), it was not clear what is most significant from the point of view of an overall model atmosphere accuracy: to compute NLTE models without influence of metal line blanketing (or with a very simplified blanketing), or to treat metal line blanketing as completely as possible, while making a sacrifice of neglecting NLTE effects.

Anderson (1985) has introduced an ingenious multifrequency/multigray method and was able to construct models with several tens to hundreds of energy levels and hundreds of lines treated explicitly. When the ALI method was first implemented (Werner 1986), the number of lines that can be treated explicitly increased to thousands. Anderson (1989) used a concept of superlevels and superlines to describe effects of numerous lines of iron peak elements. Later, even more complex model atmospheres with improved treatment of metal line blanketing were constructed (Dreizler & Werner 1993; Hubeny & Lanz 1995). The experience gained during the last decade taught us that both NLTE and line blanketing are very important; moreover, one needs to treat both to a very high degree of completeness in order to avoid spurious results.

With the recent improvements of numerical schemes and with extensive developments of computational resources that have occurred during the last decade, we are now able to compute essentially "exact," fully blanketed NLTE hydrostatic model atmospheres. To fulfill this goal is the topic of the present paper.

The paper is organized as follows. In § 2 we summarize the basic physical assumptions and the numerical methods used to construct our model grid, and in § 3 we specifically describe numerical approaches to treat the metal line blanketing. Section 4 is devoted to an overview of atomic data and, in some cases, their approximations. Section 5 describes the OSTAR2002 model grid in more detail. Some representative results are presented in § 6, while global parameters such as the number of ionizing photons and a bolometric correction are discussed in § 7. Section 8 discusses a sensitivity of computed models to adopted parameters. Our results are summarized in § 9.

2. ASSUMPTIONS AND METHODS

Our basic physical assumptions are those of plane-parallel stratification, hydrostatic equilibrium, and radiative equilibrium. As has been pointed out in the literature repeatedly over the past three decades (Auer & Mihalas 1969b; Mihalas 1978; a number of papers in Garmany 1989; Crivellari et al. 1991; Heber & Jeffery 1992; Hubeny, Mihalas, & Werner 2003), the approximation of LTE, which is another typical approximation of classical model atmospheres, breaks down for early-type stars, in particular for O stars. We thus drop the approximation of LTE and compute NLTE models.

2.1. Are Hydrostatic O Star Model Atmospheres Relevant?

At the very outset, we have to clarify one crucial question. It is well known that the most common features of the UV spectra of O stars are strong P Cygni profiles of numerous metal lines (C IV, N V, O V, Si IV, S IV, S V, P V, etc.), which provide unmistakable evidence of massive, supersonic outflows—the stellar winds. Since our models are hydrostatic, we have to ask, are the hydrostatic model atmospheres for O stars relevant at all?

The answer depends on what exactly we are expecting from a model. If we intend to analyze the P Cygni profiles and to derive basic wind parameters (mass-loss rate, terminal velocity), then, obviously, the hydrostatic models at best provide lower boundary conditions. However, if we intend to derive the basic stellar parameters (effective temperature, surface gravity [and therefore mass], and chemical composition), from the bulk of the UV and optical spectrum, then the answer is that the hydrostatic models are not only useful but in many cases actually preferable over the wind models or the unified (photosphere plus wind) models with a simplified treatment of a photosphere. There are several reasons for this assessment.

First, most spectral lines (excluding strong, mostly resonance, lines) are formed in the photosphere where velocities are small and geometrical extension is negligible. Indeed, the spectrum of slowly rotating O stars shows mostly narrow and symmetric lines (see, e.g., the high-resolution UV spectral atlas of the O9 V star, 10 Lac [Brandt et al. 1998], and the quality of the fit of the *Hubble Space Telescope* spectra by our NLTE line-blanketed models [Hubeny, Heap, & Lanz 1998]). This statement is valid in all but the most extreme cases of stellar winds, like those observed in Wolf-Rayet stars and extreme Of supergiants. Moreover, winds are weaker in low-metallicity environments, making photospheric models even more relevant in this case. The theoretical spectra predicted by the wind code CMFGEN (Hillier & Miller 1998) and by TLUSTY agree very well for a test case, $T_{\rm eff} = 35,000$ K, $\log g = 4.0$, demonstrating that most lines are indeed formed in the quasi-static photosphere (Hillier & Lanz 2001; Bouret et al. 2003).

Second, there are many remaining uncertainties as to the exact properties of stellar winds of hot stars, even though the paradigm of radiatively driven winds is well established. For example, we do not have in many cases a consistent solution: the calculated line force is often too small to drive a wind through the critical point (although some progress is being made), so a β-type velocity law must be adopted to describe empirically the velocity and density structure of the wind. Furthermore, radiative equilibrium is not really satisfied in these winds, where shocks dump mechanical energy

and heat the wind, thus changing its ionization structure (e.g., superionization). Finally, the assumption of one-dimensional geometry is challenged by the likely presence of dense clumps in the wind and by rotation; the role of magnetic fields is not yet understood, and their importance in structuring the wind will very likely be greater than in the photosphere.

Third, there is also a practical aspect. Spherical model atmospheres with velocity fields, although technically still a one-dimensional problem, have effectively a larger dimensionality than a plane-parallel static problem because of a sharp angular dependence of the radiation field. (Recall that in spherical wind models, the number of angles is about the same as the number of discretized radial points, while in the plane-parallel case considering a few [typically three] angles is usually sufficient.) Consequently, computing spherical expanding models is intrinsically more complex and more computationally intensive than plane-parallel models. One is thus forced either to compute fewer models or to make approximations in the local physics (in particular opacities), to reduce computer requirements to reasonable limits.

Finally, it is important to realize that while line blanketing operates everywhere in the atmosphere, departures from hydrostatic equilibrium occur only in the outer layers. History has taught us that it is very dangerous to neglect or even to approximate metal line blanketing. Neglecting line blanketing leads not only to a lower local temperature in the continuum-forming layers and thus to systematic errors in determining the effective temperature (e.g., Hubeny et al. 1998) but also to errors in predicted ionization balance of important elements (CNO, etc.). These species provide in turn important diagnostic tools for the wind. Since the ionization edges of CNO and other light metals are located in the far- and extreme-ultraviolet (EUV), and since this region is crowded with numerous lines of highly ionized iron and nickel (Fe IV–Fe VI; Ni IV–Ni VI), any deficiencies in describing photospheric line blanketing are directly reflected in the uncertainties in the predicted wind structure. It is thus no exaggeration to say that without a proper and detailed treatment of photospheric metal line blanketing, even sophisticated wind models may be seriously in error.

Therefore, we are on much safer ground to determine the fundamental parameters of massive stars as long as we use selected photospheric lines and avoid all uncertainties remaining with wind models. Moreover, a grid of NLTE line-blanketed model atmospheres incorporating state-of-the-art opacities will provide a sound basis for comparison to future, more realistic model atmospheres of O stars.

2.2. Numerical Methods

Over the years, we have developed a computer program called TLUSTY for computing model stellar atmospheres without assuming LTE (Hubeny 1988; Hubeny & Lanz 1992, 1995, 2003; Lanz & Hubeny 2001; Lanz, Hubeny, & Heap 2003). The program solves the basic equations: radiative transfer, hydrostatic equilibrium, radiative equilibrium, statistical equilibrium, and charge and particle conservation.

These equations are discretized in frequency and depth, which yields a set of highly coupled, nonlinear algebraic equations. We have used in this work the so-called hybrid CL/ALI method that was introduced by Hubeny & Lanz (1995). This method builds on the advantages of both ALI and complete linearization (CL). Through ALI, the mean

intensities of the radiation field are eliminated from the set of linearized equations. However, the hybrid CL/ALI method still allows us to linearize the radiation intensity at a few selected key frequencies, notably improving the convergence rate compared to a "pure" ALI approach. The hybrid CL/ALI method combines therefore the low cost of ALI while retaining a convergence rate that is similar to CL. Moreover, levels and superlevels may be grouped during the linearization step, reducing even further the number of linearized equations (Hubeny & Lanz 2003). The full statistical equilibrium is solved in a separate step, element by element, with a typical maximum number of levels around 200 per element.

Under the above assumptions, the critical ingredient of the models is a degree of completeness of the opacity sources and of the atomic/ionic energy levels treated explicitly in the statistical equilibrium equations. We shall discuss these issues in more detail in the next two sections.

3. TREATMENT OF METAL LINE BLANKETING

As we have pointed out above, NLTE line blanketing is an essential ingredient of realistic model atmospheres, determining the vertical temperature structure and the ionization structure. NLTE ionization rates are typically larger than their LTE counterparts because the radiative rates are determined by the radiation field that is emitted in deeper, hotter layers. Therefore, accurate mean intensities of the radiation field are required to evaluate correctly the NLTE ionization structure, which in turn require an accounting of all sources of opacity. When neglecting in particular the opacity of Fe lines, NLTE models predict too strong EUV/UV radiation fields and overestimate the ionization and the importance of departures from LTE. In order to construct realistic NLTE model atmospheres, we have therefore included about 100,000 individual atomic levels of over 40 ions of H, He, C, N, O, Ne, Si, P, S, Fe, and Ni in the calculations. The levels are grouped into about 900 NLTE superlevels, with populations of individual energy levels following Boltzmann statistics inside a superlevel. All individual levels in a superlevel thus share the same NLTE departure coefficient. Hubeny & Lanz (1995) discussed the concept of NLTE superlevels in detail. A total of 8000 lines of the light elements and about 2 million lines of Fe III–Fe VI and Ni III–Fe VI are accounted for in the calculations. Based on a line strength criterion, Fe and Ni lines are dynamically selected from a total of 12 million lines listed by Kurucz (1994). The numbers of NLTE levels and lines included in the model atmospheres are listed in Table 1. Details of the model atoms are given in § 4.

ALI and level grouping are two major steps toward the practical realization of NLTE line-blanketed model atmospheres. "Superlines," i.e., transitions between superlevels, are another important ingredient. A superline may involve hundreds or thousands of individual lines over a relatively broad frequency range. The resulting absorption cross section is then very complex, and a detailed representation may require a very large number of frequency points. In an early implementation of NLTE line blanketing, Hubeny & Lanz (1995) adopted the concept of opacity distribution functions (ODFs) to describe the absorption profile of superlines. The total opacity of all lines in a given transition (computed using Voigt profiles for each line) is sorted; the sorted opacities could then be represented with a limited number of frequencies,

TABLE 1
ATOMIC DATA INCLUDED IN THE NLTE MODEL ATMOSPHERES

Ion	(Super) levels	Lines	References
H I.................	9	172	
H II.................	1	...	
He I...............	24	784	1
He II...............	20	190	
He III.............	1	...	
C II.................	22	238	2
C III................	23	258	3
C IV................	25	330	4
C V.................	1	...	
N II.................	26	373	5
N III...............	32	549	2
N IV...............	23	286	3
N V.................	16	330	4
N VI................	1	...	
O II.................	29	346	6
O III...............	29	846	5
O IV...............	39	922	2
O V.................	40	610	3
O VI...............	20	330	4
O VII..............	1	...	
Ne II..............	15	83	7
Ne III.............	14	32	7
Ne IV.............	12	38	6
Ne V..............	1	...	
Si III...............	30	747	8
Si IV...............	23	306	9
Si V................	1	...	
P IV	14	19	1
P V	17	223	
P VI	1	...	
S III................	20	57	10
S IV................	15	26	11
S V.................	12	11	8
S VI................	16	147	9
S VII...............	1	...	
Fe III..............	50	1,604,934	12, 13
Fe IV..............	43	1,776,984	12, 14
Fe V...............	42	1,008,385	12, 15
Fe VI..............	32	475,750	12
Fe VII.............	1	...	
Ni III..............	36	1,309,729	12
Ni IV..............	38	1,918,070	12
Ni V...............	48	1,971,819	12
Ni VI..............	42	2,259,798	12
Ni VII.............	1	...	

REFERENCES.—(1) Martin et al. 1999. (2) Fernley et al. 1999. (3) Tully, Seaton, & Berrington 1990. (4) Peach, Saraph, & Seaton 1988. (5) Luo & Pradhan 1989. (6) V. M. Burke & D. J. Lennon 2003, unpublished. (7) K. Butler & C. J. Zeippen 2003, unpublished. (8) Butler, Mendoza, & Zeippen 1993. (9) K. T. Taylor 2003, unpublished. (10) Nahar & Pradhan 1993. (11) Mendoza et al. 1995. (12) Kurucz 1994. (13) Nahar 1996. (14) Bautista & Pradhan 1997. (15) Bautista 1996.

typically 15–30 per transition, or 30,000–50,000 frequencies for the whole spectrum. The ODF approach assumes that the background opacity changes little over the frequency range covered by the superline. Details of blends with other lines or continua are therefore lost; however, this issue should not be serious in a statistical sense since this method is designed for millions of lines of the iron peak elements. One may still unintentionally create or neglect blends between strong lines and ODFs, thus affecting the resulting model atmospheres.

We have therefore implemented a second method, opacity sampling (OS), that has the advantage of treating exactly the blends. OS is a simple Monte Carlo–like sampling of the superline cross sections. Contrary to the ODF approach, OS may miss the cores of important strong lines if too few frequency points are used. We use a variant of OS, sampling the whole spectrum at prescribed intervals in frequency. The typical sampling step is 0.75 fiducial Doppler widths of Fe. Smaller steps are occasionally used to include light elements' line cores in the frequency set as well as points around photoionization edges. Our model atmospheres are sampled with 180,000–200,000 frequency points for an O star model. While costly in terms of computing requirements, we are thus sampling the spectrum with sufficient resolution to ensure that every line is accounted for. This is the current standard mode in TLUSTY, which was used to compute this grid of model atmospheres.

Lanz & Hubeny (2003) presented some illustrations of the ODF and OS approaches. In § 8 we show the changes in a typical model atmosphere that result from different representations of line opacities.

4. ATOMIC DATA

The OP (Opacity Project Team 1995, 1997) provides very extensive data sets for radiative transitions (gf-values, photoionization cross sections) that have been obtained from ab initio calculations for all ions of the most abundant light species ($Z \leq 14$; S, Ca, and Fe). The current status of the project and its continuation as the IRON Project is discussed by Nahar (2003). The Opacity Project Team claims that their data are accurate at the 10% level or better. We have systematically adopted these data for light elements, and they form the bulk of radiative data used in TLUSTY. The OP data have been extracted from TOPbase,[2] the database of the Opacity Project (Cunto et al. 1993). OP also provides theoretical level energies. Despite the sophistication of OP calculations, these energies still differ by a few percent from the energies measured in the laboratory. We have therefore updated the level energies with experimental energies when they are available in the Atomic and Spectroscopic Database[3] at NIST (Martin et al. 1999). These large data sets are manipulated with MODION,[4] an IDL-based graphic tool that works directly with TOPbase data files to prepare the model atoms required by TLUSTY. For most lines, we have adopted depth-independent Doppler line profiles, with a standard temperature $T = 0.75T_{eff}$. Depth-dependent, Stark or Voigt profiles are used for the strongest lines (about 70 lines of light elements and the lower line series of H I and He II). Radiative damping constants are extracted from the NIST database, and Stark widths are adopted from the work of Dimitrijevic and collaborators. OP photoionization cross sections contain many autoionization resonances. As TLUSTY handles large frequency sets, we could therefore adopt the theoretical OP cross sections in every detail. However, sharp resonances are not fully resolved by the OP calculations. Moreover, resonances are shifted off their exact wavelengths as a result of the limited accuracy of theoretical energies. Therefore, we have

followed Bautista, Romano, & Pradhan (1998) and implemented the concept of resonance-averaged photoionization (RAP) cross sections. The cross sections are smoothed by a Gaussian with a width, $\delta E/E = 0.03$, that corresponds to the typical uncertainty of the resonance energies. OP photoionization cross sections are total cross sections for each initial state summed over all final states. We have kept this approximation: we assume that all bound-free transitions considered by TLUSTY end up in the ground state of the next ion. If the transition to the ground state is forbidden by selection rules, the cross sections are shifted in energy corresponding to the excitation of the lowest excited state for which the transition is allowed. While the opacity and the ionization rate are thus computed correctly, the corresponding recombination rate (based on detailed balance arguments) is only approximate because it assumes that the end state of ionization is in Boltzmann equilibrium with the ground state. Nevertheless, since the population balance of the upper ion is determined by a large number of processes (mostly bound-bound transitions), the influence of an approximate recombination rate is typically small and the resulting error in the statistical equilibrium virtually negligible. Additional details on the model atoms for each ion are given in the relevant subsections.

For iron peak elements, we have extracted level energies and line oscillator strengths from Kurucz (1994) extensive semiempirical calculations. Kurucz (1994) lists thousands of energy levels for each ion. A statistical approach to deal with so many levels is therefore necessary; solving the full statistical equilibrium equations would indeed require inverting very large matrices, which is not only costly but numerically inaccurate. We therefore group individual levels into superlevels, assuming that the population of each level in a given superlevel follows the Boltzmann distribution. While the populations of superlevels could depart from their LTE values, all sublevels in a given superlevel share the same b-factor. We have applied two criteria to group the levels: all sublevels must have very close excitation energies, and they must share the same parity. The first criterion ensures that collisional rates between sublevels are large enough to achieve the Boltzmann statistics; the second criterion further supports the validity of this assumption by treating properly transitions out of and into metastable states. The second requirement provides the additional advantage of avoiding radiative transitions within a single superlevel. The absorption cross section of a superline between two superlevels can be quite complex, involving hundreds or thousands of individual lines. Exact absorption cross sections are computed at three depths (top and bottom of the model atmosphere, and at a depth where $\tau_{\mathrm{Ross}} \approx 1$ and $T \approx T_{\mathrm{eff}}$) and are logarithmically interpolated between these points. A detailed representation requires a very large number of frequency points. OS is a method designed for handling such cases, and its implementation in TLUSTY was outlined in § 3.

NLTE calculations also require collisional excitation and ionization rates. However, collisional rates are known only for a limited set of transitions, mostly intersystem transitions that are important for diagnostics at low densities. The IRON Project (Hummer et al. 1993) is starting to remedy this situation, but their data are not yet implemented in TLUSTY. We rely on general formulae at this stage. We use the Seaton (1962) formula for collisional ionization; for optically allowed line transitions, we use the van

Regemorter (1962) formula, which is accurate to about 30%–50% (A. K. Pradhan 2000, private communication); for forbidden transitions, no approximate formula or simple prescription is available, so we somewhat arbitrarily use Eissner-Seaton's formula with $\gamma(T) = 0.05$. Different approaches of collisional strengths in superlines may be implemented. Lanz & Hubeny (2003) compared two different estimates and argued that the most natural way consists of summing up all contributions for individual transitions, using the appropriate formulae for allowed and forbidden transitions. We have adopted this approach here.

The following subsections provide the relevant details of the model atoms. Table 1 summarizes the atomic data included in the model atmospheres, as well as the references to the original calculations collected in TOPbase. Data files and Grotrian diagrams may be retrieved from the TLUSTY Web site[5].

4.1. Hydrogen

The model atom of hydrogen includes the lowest eight levels and one superlevel grouping the higher excitation levels, from $n = 9$ to 80, following the occupation probability formalism developed by Hummer & Mihalas (1988) and extended to NLTE situations by Hubeny, Hummer, & Lanz (1994). The Lyman and Balmer continuum cross sections are generalized to account for transitions from these two levels to dissolved higher states. This contribution is neglected for all other continua.

All lines between the first eight bound levels are included, assuming an approximate Stark profile for the Lyman and the Balmer series (Hubeny et al. 1994) and a Doppler profile for the other lines. The higher members of the Lyman and the Balmer line series are incorporated via the OS approach. This is the only difference from the treatment of Hubeny et al. (1994), who adopted ODFs. OS is used here in order to account exactly for line blending with the He II line series (and with other lines). Higher members of other line series are neglected.

Hydrogen is the main opacity source in the photospheres of O stars. We can benefit most from our hybrid CL/ALI method by selecting a few key frequencies where the hydrogen opacity is largest, at which the mean intensity of the radiation field is linearized. We have selected the first six frequencies immediately higher than the Lyman edge, the three core frequencies in Lyα, and the core frequency of Lyβ, Lyγ, Hα, and Hβ. A few more frequencies have been selected in the cores of strong resonance lines of other species and will be mentioned in the relevant subsections. Although there might be a different optimal choice of these frequencies for each individual model atmosphere, we have found that this choice was generally adequate to achieve most of the gains of the CL/ALI method in the parameter space covered by the OSTAR2002 grid.

4.2. Helium

Neutral helium is modeled with a 24-level atom, which incorporates all 19 individual levels up to $n = 4$ and five superlevels grouping levels with identical principal quantum numbers ($5 \leq n \leq 8$); for $n = 5$, singlet and triplet levels are grouped into two separate superlevels. We have performed some tests with more detailed model atoms, splitting the

---

[5] Available at http://tlusty.gsfc.nasa.gov.

superlevels up to $n = 6$, or including higher excitation levels, but we did not find significant differences. All lines from $n \leq 4$ levels are included, but infrared lines between high-excitation levels ($n \geq 5$) are assumed to be in detailed radiative balance. Voigt line profiles are used for lower excitation lines ($n \leq 2$), and Doppler profiles are assumed for higher excitation lines. He I is treated in a special way in TLUSTY; like hydrogenic ions, and contrary to all other ions, we have special subroutines in the code to deal with atomic data. We use D. G. Hummer's (1988, private communication) routine to evaluate the photoionization cross sections; the routine is based on Seaton & Fernley's cubic fits of OP data and properly manages the different ways of averaging levels. Bound-free and bound-bound collisional transitions rates are also evaluated with a special routine based on approximate expressions from Mihalas, Heasley, & Auer (1975). For bound-bound transitions between low-excitation levels, these approximate rates are superseded by detailed calculations of collisional cross sections (Berrington & Kingston 1987), used by P. J. Storey & D. G. Hummer (1988, private communication) to evaluate collisional rate coefficients.

The ionized helium model atom includes the first 20 bound levels. The He II model is built following closely H I. We will only indicate here the differences. The occupation probability formalism (Hubeny et al. 1994) is taken into account for the 20 bound levels, but higher excitation levels are not included explicitly. We also use continuum cross sections for bound-free transitions from the ground and first excited levels that account for transitions to highly excited, dissolved levels. Stark profiles are adopted for the first four line series, while infrared lines ($n > 10$) are set to detailed radiative balance. Finally, the first three frequencies at the head of the He II Lyman continuum are linearized in the ALI/CL scheme.

4.3. Carbon

The general handling of atomic data has been discussed at the beginning of § 4. We restrict the following subsections to a few particulars relative to each ion. Carbon is represented by a 22-level C II model atom, a 23-level C III model atom, and a 25-level C IV model atom, grouping 44, 55, and 55 individual levels, respectively. The C II model atom includes the first 17 levels, 14 from the doublet system and the first three levels of the quartet system. Five superlevels group higher excitation levels, four in the doublet system ($6 \leq n \leq 9$) and one superlevel grouping three levels in the quartet system. The C III model atom includes the first 16 levels ($E \leq 312,000$ cm^{-1}) and groups all higher excitation levels up to $n = 6$ into seven superlevels. Levels with $n \geq 7$ are not included explicitly (see further discussion in § 8 about this restriction and its consequence on C^{+3} recombination). The C IV model atom includes all individual levels up to $n = 6$ and four superlevels ($7 \leq n \leq 10$). The data extracted from TOPbase have been extended to include all levels up to $10m$ $^2M^0$. We have included the two fine-structure levels of $2p$ $^2P^0$ for an exact treatment of the C IV $\lambda 1549$ resonance doublet. Depth-dependent Voigt profiles are adopted for the resonance lines of the three ions and for the strong C III $\lambda 1176$ line from the $^3P^0$ metastable level.

4.4. Nitrogen

The model atmospheres incorporate four ions of nitrogen, N II–N V, and the ground state of N VI. The first 16 levels in the singlet and triplet systems of N II ($n = 2$; $3s$ and $3p$ levels) and the first two quintet levels are included in the models as explicit individual NLTE levels. Higher excitation levels ($3d$; $4 \leq n \leq 5$) are grouped into eight superlevels, four in each system. Higher levels ($n \geq 6$) are not incorporated explicitly in the model atom. The N III model atom includes all the levels below the ionization limit as extracted from TOPbase. The first 24 levels ($E \leq 330,000$ cm^{-1}) are treated as individual levels, and the other 43 levels are grouped into seven superlevels. The ground state is split into two fine-structure levels for an exact treatment of the resonance doublets (e.g., N III $\lambda 990$). The N IV model atom was constructed similarly to the C III model atom. The first 15 levels are included explicitly, and higher levels up to $n = 6$ are grouped into eight superlevels. Levels with $n \geq 7$ are not included explicitly. Finally, the N V model atom is similar to C IV, although levels are grouped into six superlevels starting with $n = 5$ levels. The two fine-structure levels of $2p$ $^2P^0$ are included in the model atom. Depth-dependent Voigt profiles have been set up for 18 resonance lines of the four ions.

4.5. Oxygen

The model atmospheres incorporate five ions of oxygen, O II–O VI, and the ground state of O VII. O II and O III have a relatively rich structure of levels. High-excitation levels have thus not been incorporated in the model atoms. The O II model atom includes 21 individual levels and eight superlevels, grouping levels up to $n = 5$, while the O III model atom includes the lowest 20 levels and groups higher excitation levels up to $n = 6$ into nine superlevels. All O IV below the ionization limit are incorporated, the first 30 as individual levels and the others grouped into eight superlevels. Fine structure of the O IV ground state is included. The first 34 O V levels are included explicitly, and higher levels up to $n = 7$ are grouped into six superlevels. Finally, the O VI model atom is similar to C IV, although levels are grouped into five superlevels starting with $n = 6$ levels. The two fine-structure levels of $2p$ $^2P^0$ are included in the model atom. Depth-dependent Voigt profiles have been set up for O IV $\lambda\lambda 789, 609, 554$, and O V $\lambda 630$.

4.6. Neon

Simple model atoms have been built for the neon ions, Ne II–Ne IV. We are not aiming at a detailed NLTE calculation of Ne populations, but our purpose was to account for the bound-free opacity in the EUV due to the ionization of this abundant species. The Ne II model atom includes the first 11 levels and groups levels up to $E \leq 300,000$ cm^{-1} into four superlevels. Ne III levels up to $E \leq 400,000$ cm^{-1} are included in the model atom, as 12 individual levels and two superlevels. Finally, the Ne IV model atom includes the first 10 levels and two superlevels grouping levels up to $E \leq 550,000$ cm^{-1}. All lines are assumed to have depth-independent Doppler profiles.

4.7. Silicon

Detailed model atoms have been constructed for Si III and Si IV because the silicon ionization balance is a good temperature indicator for late O and B stars. The Si III includes all 105 energy levels listed by TOPbase below the ionization limit. The first 24 levels are treated as individual explicit levels, while the higher levels are grouped into six superlevels

(three superlevels in the singlet and in the triplet systems). The Si IV model atom includes all individual levels up to $n = 6$ and four superlevels ($7 \leq n \leq 10$). The data extracted from TOPbase have been extended to include all levels up to $10m\ ^2M^0$. We have included the two fine-structure levels of $2p\ ^2P^0$ for an exact treatment of the Si IV $\lambda1397$ resonance doublet. Depth-dependent Voigt profiles are adopted for Si III $\lambda\lambda1206, 567$ and Si IV $\lambda\lambda1394, 1403$ resonance lines.

4.8. *Phosphorus*

Phosphorus has not been considered by OP because the relatively low phosphorus abundance in the Sun indicates that phosphorus is most likely only a minor contributor to the total opacity in astrophysical plasmas. However, we have included phosphorus as an explicit NLTE species in our model atmospheres as a result of the potential diagnostic value of the P IV $\lambda951$ and P V $\lambda\lambda1118$–1128 resonance lines. We have built simple model atoms based on data extracted from the NIST Atomic and Spectroscopic Database. The P IV model atom includes the first 14 levels, while the P V model atom includes individual levels up to $n = 5$ and groups $6 \leq n \leq 9$ levels into four superlevels. We have approximated the photoionization cross sections by interpolating in cross sections from the same configurations in isoelectronic sequences (e.g., using Si IV and S VI cross sections to estimate P V cross sections). We believe that this approach is likely more realistic than a simple hydrogenic approximation.

4.9. *Sulfur*

The model atmospheres incorporate four ions of sulfur, S III–S VI, and the ground state of S VII. The model atoms are kept relatively simple, aiming at including the sulfur bound-free opacity in the model atmospheres and at predicting a few key diagnostics lines, mostly S IV $\lambda1073$ and S V $\lambda1502$. The S III model atom includes all levels with $E \leq 200,000$ cm^{-1}, the first 16 levels individually and the other 11 levels grouped into four superlevels. The S IV model atom includes the first 14 levels up to $E \leq 225,000$ cm^{-1}, while the S V model atom includes the first 12 levels. The S VI model atom includes all individual levels up to $n = 5$ and three superlevels ($6 \leq n \leq 8$). Fine structure of S IV and S VI $3p\ ^2P^0$ levels is taken into account. The S VI $\lambda\lambda933$–945 resonance lines are the only sulfur lines for which we have adopted depth-dependent Voigt profiles.

4.10. *Iron*

The model atoms of iron peak elements are based on Kurucz (1994) extensive semiempirical calculations. We have extracted a list of even- and odd-parity levels for each ion included in the model atmospheres. We have considered all levels, those with experimental energies as well as those with predicted energies. We plotted histograms of numbers of levels per energy interval to set up the energy bands defining the superlevels. We chose typically 15–30 bands per parity, so the model atoms have 30-50 superlevels. For each ion, we read the full line list from Kurucz (1994) and select dynamically the strongest lines. The line selection criteria include line gf-values, excitation energies, and ionization fractions. In this way, we skip most or all Fe VI lines in the coolest models and most or all Fe III lines in the hottest models. We have extracted photoionization cross sections from the latest calculations of Fe III–Fe V by the Ohio State group (see Table 1). They assumed LS coupling, and we could typically assign theoretical cross sections to observed levels for the lowest 20–30 levels. We have assumed a hydrogenic approximation for higher excitation levels and for all Fe VI levels. The data were then summed up to set up cross sections for the superlevels. Finally, we have applied to these cross sections the RAP smoothing technique.

4.11. *Nickel*

We have followed the same approach for nickel, using Kurucz (1994) data. OP did not include nickel in their calculations. We have therefore adopted a hydrogenic approximation for the photoionization cross sections.

5. DESCRIPTION OF THE GRID

The OSTAR2002 grid covers the parameter space of O stars in a dense and comprehensive way. We have selected 12 effective temperatures, $27,500$ K $\leq T_{\rm eff} \leq 55,000$ K, with 2500 K steps, eight surface gravities, $3.0 \leq \log g \leq 4.75$, with 0.25 dex steps, and 10 chemical compositions, from metal-rich relative to the Sun to metal-free. Table 2 lists the selected metallicities. Solar abundances refer to Grevesse & Sauval (1998). In every case, we have assumed a solar helium abundance, He/H $= 0.1$ by number. All other chemical abundances are scaled from the solar values. TLUSTY can readily accommodate non–solar-scaled abundances resulting, e.g., from mixing of CNO cycle processed material; however, this would increase the total number of models to compute to an unmanageable level by increasing the dimensionality of the parameter space. Thus, we view this grid as a starting point from which detailed abundance analyses can be performed. The selected chemical compositions have been chosen to cover a number of typical environments of massive stars: the Galactic center (" C models "), the Magellanic Clouds (" L models " for LMC; " S models " for SMC), blue compact dwarf galaxies (e.g., " W models " for I Zw 18), and galaxies at high redshifts (" X and Y models ").

For each composition, we have computed 68 model atmospheres, as illustrated in Figure 1. Evolutionary tracks from the Geneva group (Schaller et al. 1992; Charbonnel et al. 1993) have been overplotted in Figure 1. Stars with masses larger than about 15 $M_\odot$ are in the range covered by our model atmospheres. The highest gravity and the lowest temperature have been included in the grid to avoid extrapolations when using this grid as a starting point for NLTE spectral analyses.

The lower limit in $\log g$ is set by the Eddington limit. Using NLTE H-He model atmospheres, we have estimated the lowest surface gravity as a function of $T_{\rm eff}$, which would correspond to the Eddington limit neglecting the effect of

TABLE 2
KEY TO MODELS AND CHEMICAL COMPOSITIONS

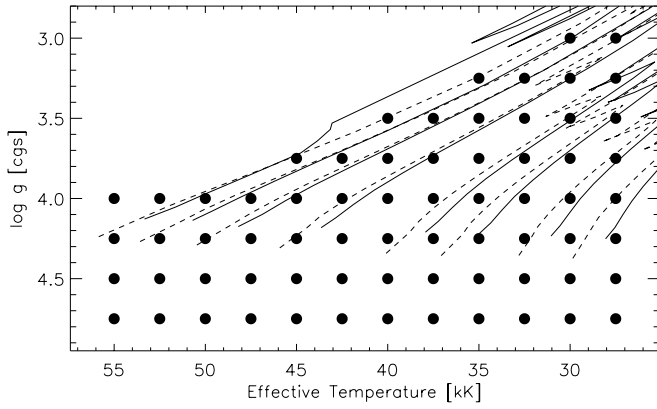| Key	Composition	Key	Composition
C..........	$2 \times \odot$	V..........	$1/30 \times \odot$
G	$1 \times \odot$	W.........	$1/50 \times \odot$
L..........	$1/2 \times \odot$	X..........	$1/100 \times \odot$
S	$1/5 \times \odot$	Y..........	$1/1000 \times \odot$
T..........	$1/10 \times \odot$	Z..........	0

FIG. 1.—Selected OSTAR2002 grid points in the $\log g$–$T_{\rm eff}$ plane. Geneva evolutionary tracks (Schaller et al. 1992; Charbonnel et al. 1993) are shown for solar (*solid lines*) and $\frac{1}{5}$ solar metallicities (*dashed lines*). The tracks correspond to models with initial masses of 120, 85, 60, 40, 25, 20, 15, and 12 $M_\odot$, from left to right.

FIG. 3.—Isolines of radiative acceleration relative to gravitational acceleration, $\Gamma_{\rm rad} = g_{\rm rad}/g$, for solar composition model atmospheres, as a function of $T_{\rm eff}$ and $\log g$. $\Gamma_{\rm rad}$ values are listed to the right of the isolines. The dashed line shows an estimate of the Eddington limit obtained by extrapolation.

rotation. This limit is reached for values typically 0.1–0.2 dex smaller than the grid limit. We present in Figure 2 the variation of the radiative acceleration with depth for a solar composition model, $T_{\rm eff} = 40,000$ K, and $\log g = 4.0$. The radiative acceleration goes through a maximum in the continuum-forming region ($\tau_{\rm Ross} \approx 1$) and shows a strong increase in very superficial layers ($\tau_{\rm Ross} \leq 10^{-6}$). Near the surface, this model atmosphere becomes unstable ($g_{\rm rad} > g$). Our modeling assumptions obviously break down in these layers. We have therefore numerically limited the radiative acceleration in superficial layers to ensure convergence. This case is quite typical; a similar behavior is observed in all our model atmospheres, although higher gravity models remain numerically stable at every depth (about two-thirds of all solar composition models). The model spectra are not affected by this approximation because these superficial layers only influence the strong resonance lines that form in a stellar wind. The stability of our model atmospheres is defined by the maximum reached by
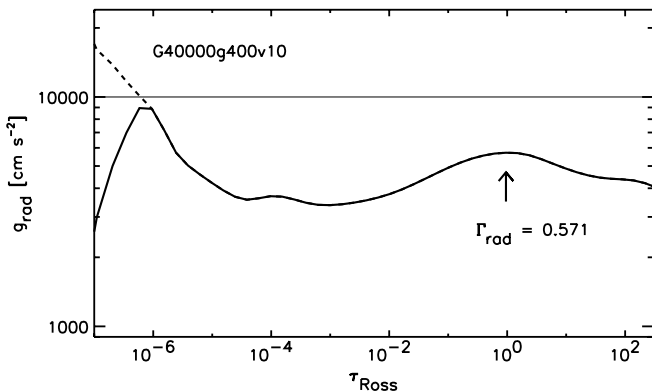
the radiative acceleration in the photosphere (see Fig. 2). Figure 3 displays contours of this maximum relative to the gravitational acceleration, $\Gamma_{\rm rad} = \max(g_{\rm rad})/g$, as a function of effective temperature and gravity. Models tend to become numerically unstable when $\Gamma_{\rm rad} > 0.9$, thus setting limits to our grid. Static model atmospheres are increasingly unrealistic so close to the Eddington limit ($\Gamma_{\rm rad} = 1$).

Finally, we have always adopted a microturbulent velocity, $\xi_t = 10$ km s^{-1}, which is a value typically found in spectral analyses of O stars. These analyses have been performed with static model atmospheres, as well as with wind codes. Bouret et al. (2003) found that TLUSTY and CMFGEN models require similar microturbulent velocities to match the UV metal lines in SMC O dwarfs, showing therefore that microturbulence is not an artifact of static model atmospheres but that it indicates the presence of additional nonthermal motions in the atmosphere. We have included the resulting turbulent pressure term in the hydrostatic equilibrium equation.

5.1. *Output Products and Availability*

The model atmospheres are available from the TLUSTY Web site (see footnote 2). Each model is characterized by a unique file name describing the parameters of the model, for example, G35000g400v10. The first letter indicates the composition (see Table 2), followed by the effective temperature, the gravity, and the turbulent velocity. Each model comes as a set of six files, with an identical file name's root but a different extension. A complete description of the files' content and format can be found in the TLUSTY User's guide (see TLUSTY Web site; footnote 2); for reference, we describe them only very briefly here:

FIG. 2.—Radiative acceleration (*thick line*) for a solar composition model atmosphere, $T_{\rm eff} = 40,000$, $\log g = 4.0$. At low optical depths ($\tau_{\rm Ross} < 10^{-6}$), the total radiative acceleration (*dashed line*) increases and becomes larger than the gravitational acceleration (*thin line*). We apply a numerical cutoff to the radiative acceleration to ensure convergence. The assumption of hydrostatic equilibrium breaks down in these superficial layers. The arrow indicates our definition of stability against radiation pressure ($\Gamma_{\rm rad} < 1$).
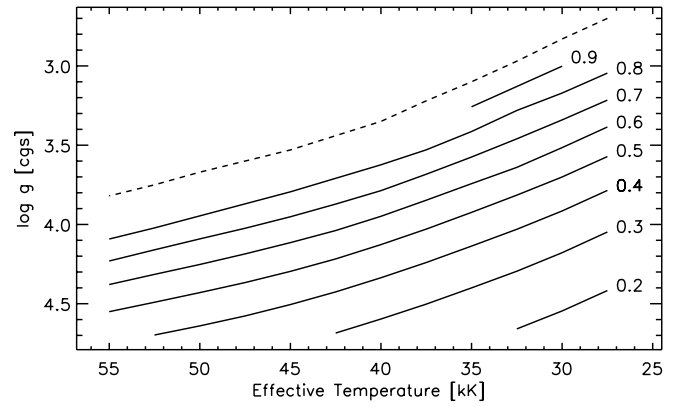
  1. model.5: general input data;
  2. model.nst: optional key words;
  3. model.7: model atmosphere: temperature, electron density, total density, and NLTE populations as function of depth;
  4. model.11: model atmosphere summary;
  5. model.12: model atmosphere: similar to model.7, but NLTE populations are replaced by *b*-factors;

6. model.flux: model flux distribution from the soft X-ray to the far-infrared given as the Eddington flux[6] H_ν (in ergs s^{-1} cm^{-2} Hz^{-1}) as function of frequency.

The model fluxes are provided at all frequency points included in the calculations (about 180,000–200,000 points with an irregular sampling). Additionally, we have computed detailed emergent spectra with SYNSPEC, version 45, in the far-UV (900–2000 Å) and in the optical (3000–7500 Å). File name extensions are model.uv.7 and model.vis.7, respectively, as well as *.17 for the continuum spectra. Only the optical spectra have been computed for the metal-free model atmospheres (model.hhe.7, model.hhe.17). Additional spectra in other wavelength ranges, with altered chemical compositions or with different values of the microturbulent velocity, can be readily computed using SYNSPEC. This requires three input files, model.5, model.7, and model.nst, and the necessary atomic data files (model atoms and the relevant line list).

5.2. *Interpolation in the Grid*

A grid of model atmospheres is a good starting point for stellar spectroscopic analyses. We can use it to study trends in spectral features with stellar parameters. However, the grid sampling is limited by the total number of model atmospheres that can be computed in some finite period of time. Therefore, we often have to resort to interpolation in the grid for analyzing individual stars. Since radiative transfer and the complete model atmosphere problem are highly nonlinear problems, interpolation will result in some errors. We need to estimate these errors and find the best way to interpolate in the grid. Here we consider two possibilities: (1) we interpolate the model atmosphere (i.e., the temperature and density stratification, as well as the NLTE populations), and then we recompute a spectrum with SYNSPEC, or (2) we interpolate directly the detailed spectra, weighted by $(T_{\rm eff}^i/T_{\rm eff}^0)^4$. The four models and spectra are otherwise given the same weight.

The OSTAR2002 grid is already finely sampled. We decided therefore to estimate the interpolation errors by comparing the "exact" UV and optical spectra with spectra interpolated following the two outlined procedures. We have performed this test on three models, S32500g350v10, L42500g400v10, and G50000g425v10. We use the four neighboring models (± 2500 K, ± 0.25 dex) to obtain the interpolated spectra. In practice, the interpolated model will always be closer to a grid point than in these test cases, which might therefore be viewed as worst cases.

The two interpolations provide spectra almost identical to the "exact" spectra. The full, detailed comparison requires too much space to appear here, but the figures are available at the TLUSTY Web site (see footnote 2). Minor differences are still found. For example, the spectrum interpolation results in a few lines being predicted too strong, especially in the S32500g350v10 case. These lines are much stronger in the coolest model spectrum as a result of lower ionization, and this demonstrates the limit of linear spectrum interpolation. On the other hand, we found that the model atmosphere interpolation results in too strong N III $\lambda 4640$ emissions in the L42500g400v10 models. These emission lines are very sensitive to the exact b-factor ratios, and small differences related to interpolations may result in

larger spectral changes. Based on these limited tests, we may however conclude that the two interpolation procedures appear both reasonably safe because of the sufficiently dense sampling of the OSTAR2002 grid. Nevertheless, we feel that model atmosphere interpolation followed by recomputing the spectrum with SYNSPEC remains the safer choice.

The same helium abundance, solar-scaled compositions, and microturbulent velocity have been adopted for all OSTAR2002 models. SYNSPEC spectra can nevertheless be recomputed with different abundances or microturbulence, using a model atmosphere with the appropriate stellar parameters. As long as these new values are not changing drastically the overall opacity and thus potentially changing the atmospheric structure, this procedure should result in realistic spectra.

6. REPRESENTATIVE RESULTS

In this section we show a few representative results. Our aim here is not to provide a comprehensive display of various models, but instead to show basic trends of important model parameters (temperature structure, emergent spectra) with effective temperature, surface gravity, and metallicity.

Figure 4 shows the local temperature for a constant surface gravity ($\log g = 4$), for three values of $T_{\rm eff}$ (30,000,
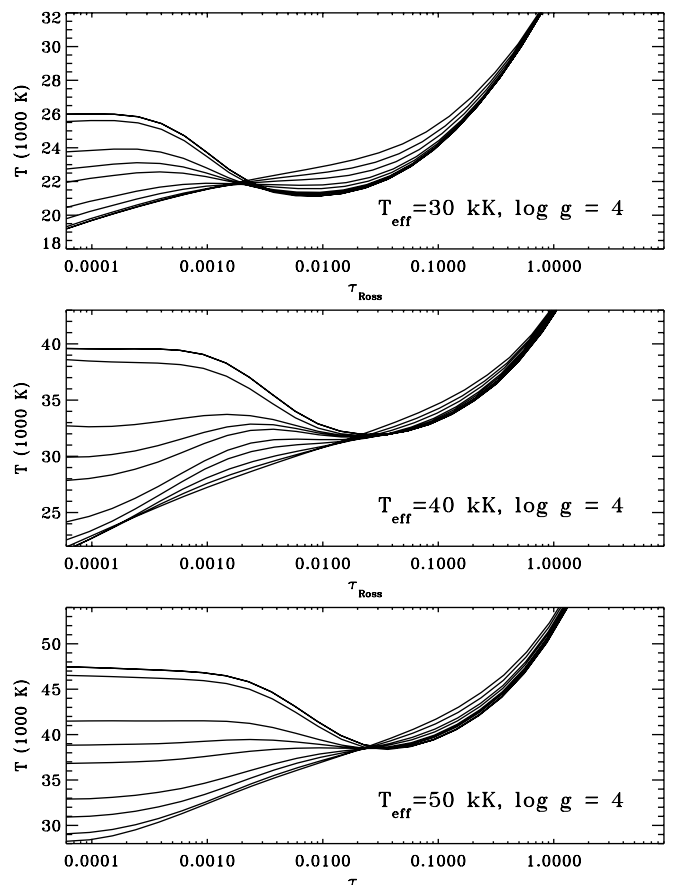
Fig. 4.—Model atmospheres for $T_{\rm eff} = 30,000$ (*top*), 40,000 (*middle*), and 50,000 K (*bottom*), $\log g = 4.0$, and various metallicities. At low optical depths ($\tau_{\rm Ross} < 10^{-3}$), the top curves are for an H-He model, and the temperature is progressively lower when increasing the metallicity, while the reverse is true at deeper layers ($\tau_{\rm Ross} > 10^{-2}$).

---

[6] The flux at the stellar surface is $F_\nu = 4\pi H_\nu$.

40,000, and 50,000 K), and for all values of metallicity. The temperature distribution nicely illustrates the basic features of line blanketing, namely, the back-warming (line blanketing leads to a heating of an atmosphere roughly between Rosseland optical depth 0.01 and 1) and the surface cooling. The zero-metallicity and very low metallicity models exhibit a temperature rise at the surface, a typical NLTE effect (an indirect heating effect of hydrogen Lyman and Balmer lines), discovered and explained already in early days of NLTE model atmospheres by Auer & Mihalas (1969a). This effect competes with surface cooling due to metal lines. At 50,000 K, both effects nearly cancel at metallicity 1/50 of solar, while at lower $T_{\rm eff}$ the rise is wiped out at higher metallicities (around 1/10 of solar). Interestingly, the temperature curves for all metallicities cross in a narrow range of optical depths; this crossing depth decreases with decreasing $T_{\rm eff}$ (being about 0.025 at 50,000 K, 0.02 at 40,000 K, and 0.002 at 30,000 K).

Figures 5–9 display the ionization fractions of all explicit species, along with LTE fractions (for a direct comparison, the LTE fractions are computed by the Saha formula for temperature and density distributions of the NLTE models; that is, we did not recompute self-consistent LTE model structures). The behavior of individual species is different,

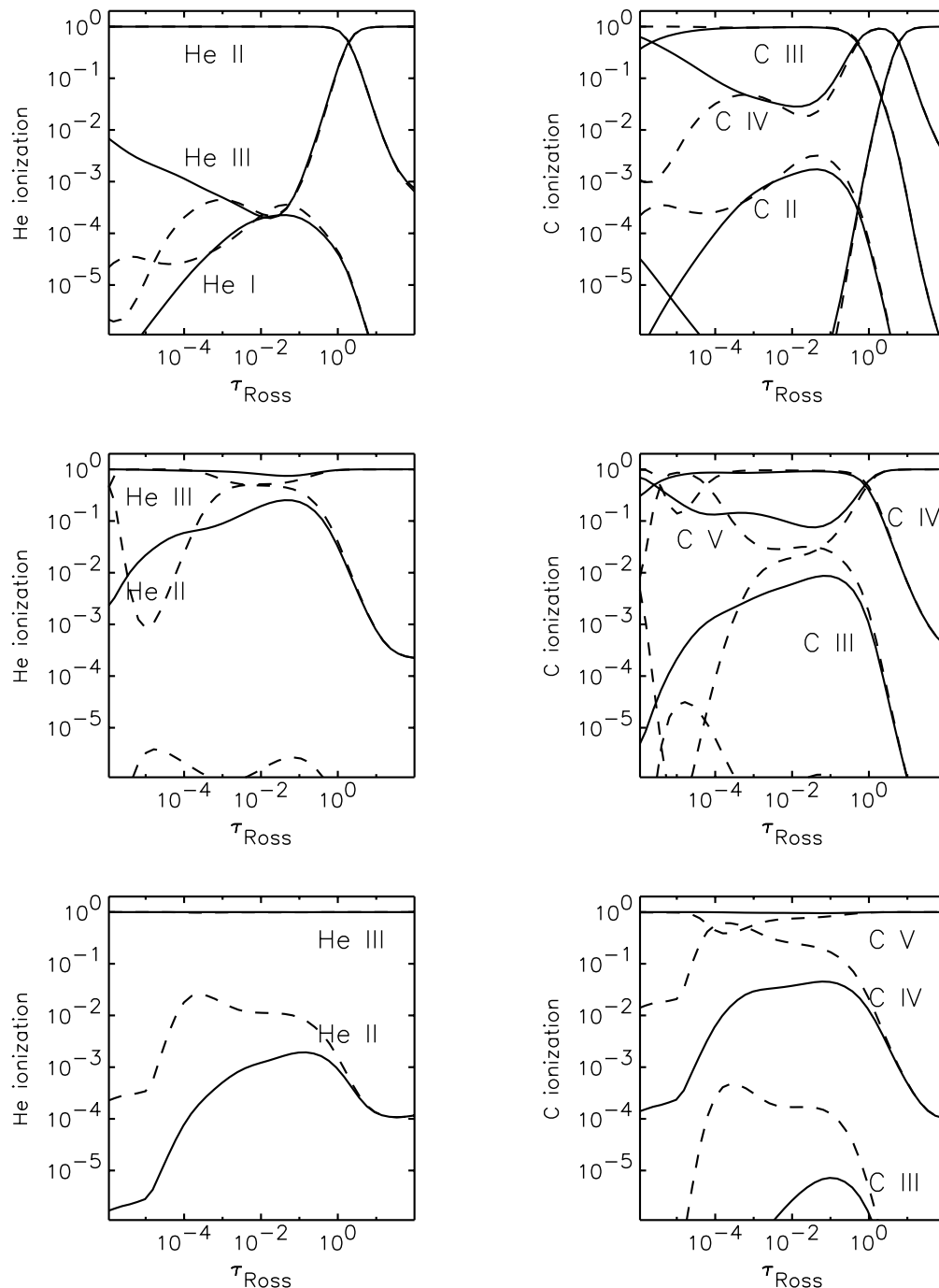Fig. 5.—Ionization fractions of helium and carbon in three model atmospheres, $T_{\rm eff} = 30{,}000$ (*top*), 40,000 (*middle*), and 50,000 K (*bottom*), log $g = 4.0$, and solar composition. LTE ionization is shown with dashed lines.
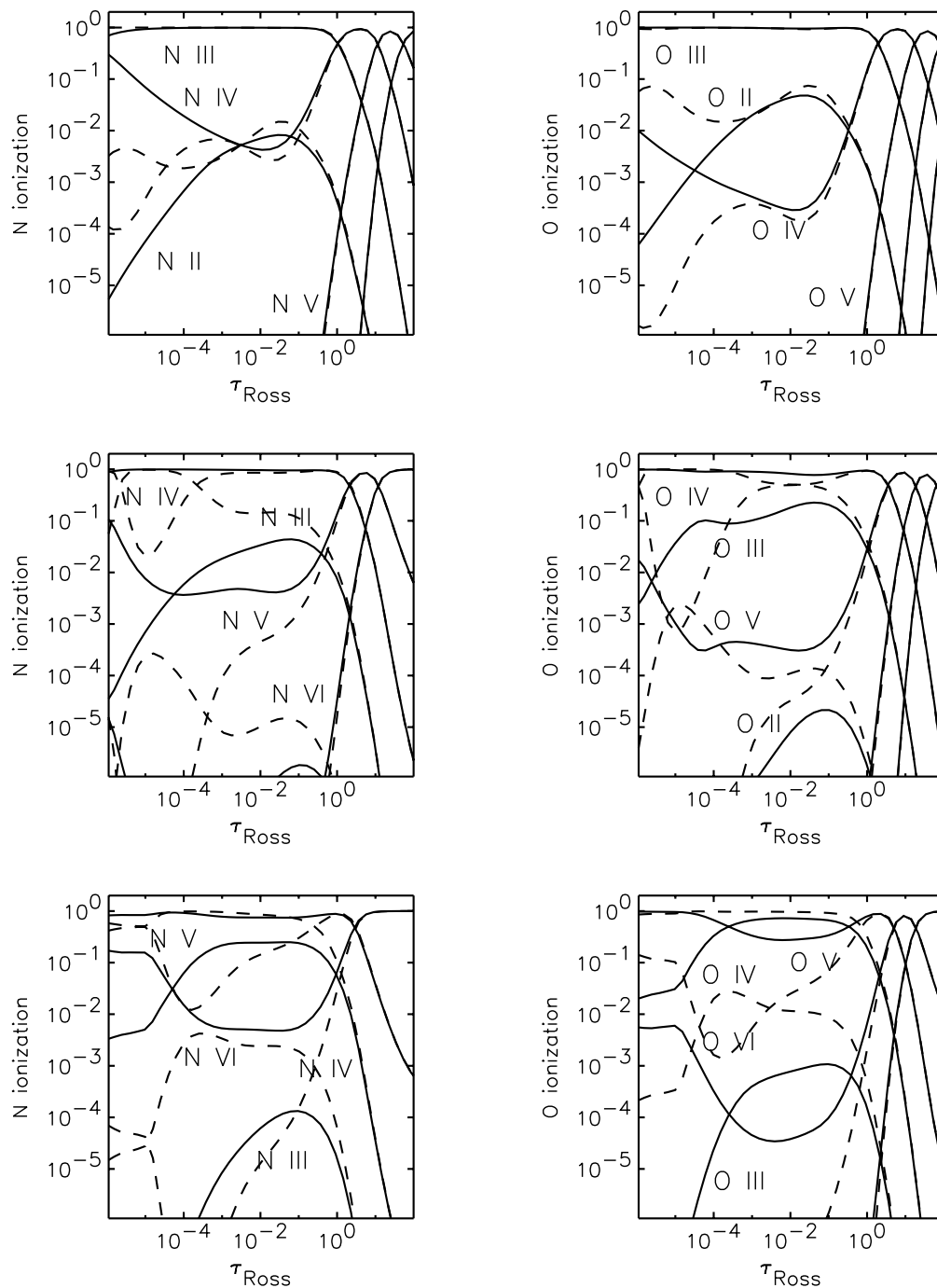
Fig. 6.—Same as Fig. 5, except for nitrogen and oxygen

but we can see a general trend: the fractions of dominant ions are usually not sensitive to NLTE effects (that is, they are close to unity in both LTE and NLTE). The fractions of ions with lower ionization degrees are typically lower in NLTE because these ions are overionized by the strong radiation field that originates in deep, very hot layers (notice that the recombination rate is given through the local temperature). Conversely, higher ionization degrees are typically larger in NLTE. This ionization shift is one of the most important NLTE effects in hot star atmospheres.

Next, we study a sensitivity of emergent flux on T_{eff}, $\log g$, and metallicity. For simplicity, we display spectra computed

directly by TLUSTY (files model.flux described earlier), not detailed spectra computed by SYNSPEC. For clarity, the spectra are smoothed over 500 frequency points, which roughly simulates a 10 Å resolution of Kurucz (1993) model spectra.

Figure 10 shows a sequence of model UV spectra with $\log g = 4$ and solar metallicity, for various effective temperatures. The Lyman jump gradually weakens with increasing effective temperature and essentially disappears at 50,000 K. Similarly, one can easily observe gradual weakening and ultimate disappearance of the Si IV $\lambda 1400$, C III $\lambda\lambda 1176$, 977, Lyα, etc., features. Figure 11 shows the effect of surface
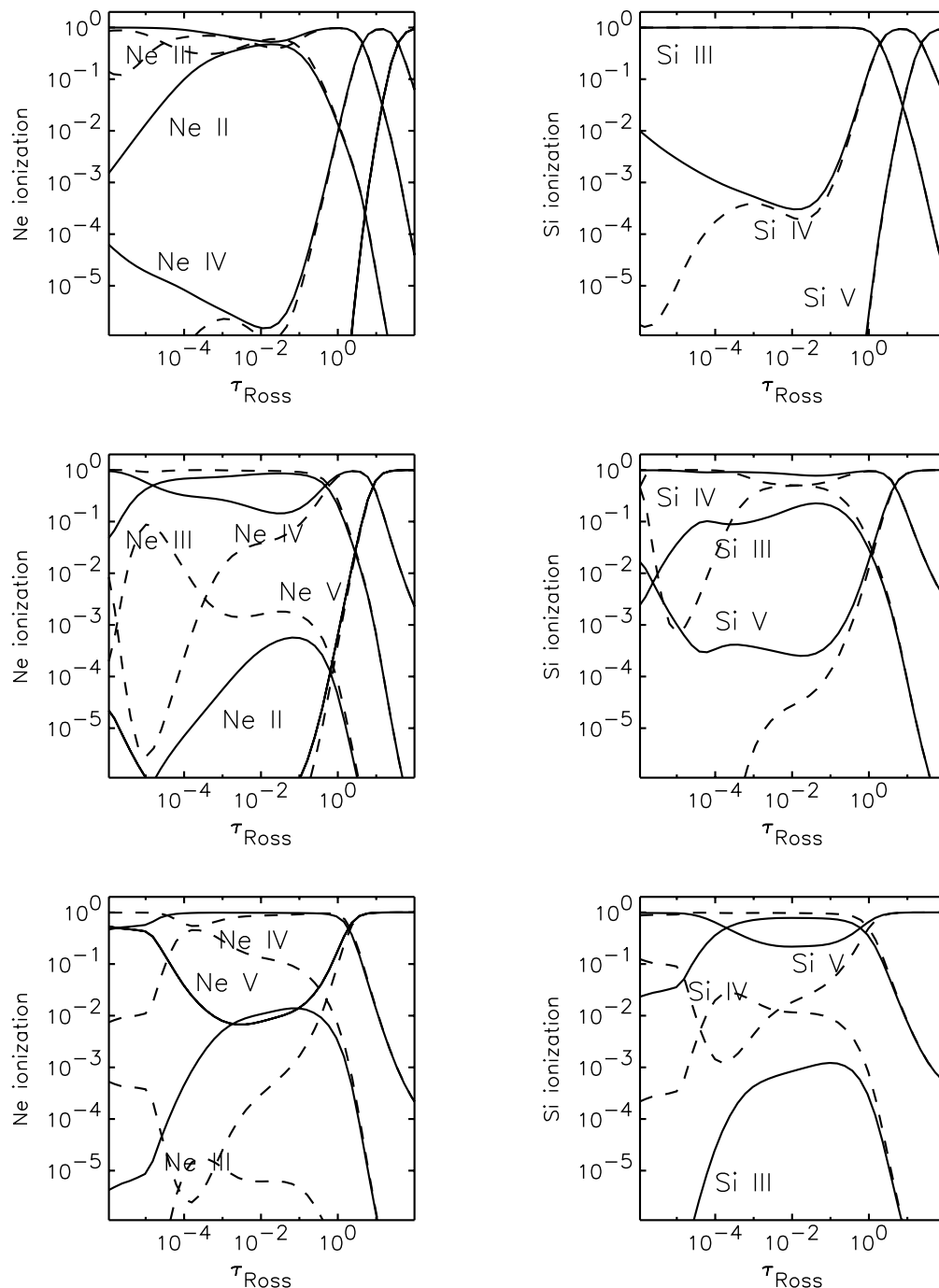
FIG. 7.—Same as Fig. 5, except for neon and silicon

gravity for a given effective temperature (40,000 K) and metallicity (solar). The most striking feature is the magnitude of the Lyman jump, which is very strong at $\log g = 4.5$ and almost disappears at $\log g = 3.5$. Similarly, the line strengths vary significantly. Next, we show the effect of metallicity. Figure 12 displays models for $T_{\mathrm{eff}} = 40,000$ K, $\log g = 4$, and metallicities $Z/Z_\odot = 2, 1, 0.5, 0.3$, and 0.1. In the low-metallicity models, the Lyman continuum flux and the near-UV continuum flux ($\lambda > 1700$ Å) are lower than those for higher metallicities. This relation is reversed in the region crowded with metal lines, 900 Å $\leq \lambda \leq 1700$ Å.

Finally, we compare our model fluxes to Kurucz (1993) models. Because of different averaging procedures used in

both sets of model spectra, the comparison is not exact but nevertheless shows the general effect. We compare three models for (T_{eff}, $\log g$) pairs equal to (40,000, 4.5), (35,000, 4.0), and (30,000, 4.0), as well as for solar metallicity (Fig. 13). The agreement between our and Kurucz models is very good in the optical spectrum for all three models (*bottom panel*). For $T_{\mathrm{eff}} = 30,000$ K the agreement between OSTAR2002 and Kurucz fluxes is rather good in the UV spectrum ($\lambda > 900$ Å), while for the hotter models our NLTE flux is lower. In contrast, NLTE models predict higher flux than Kurucz models in the Lyman continuum, although the effect is relatively small at 40,000 K (see also § 7).
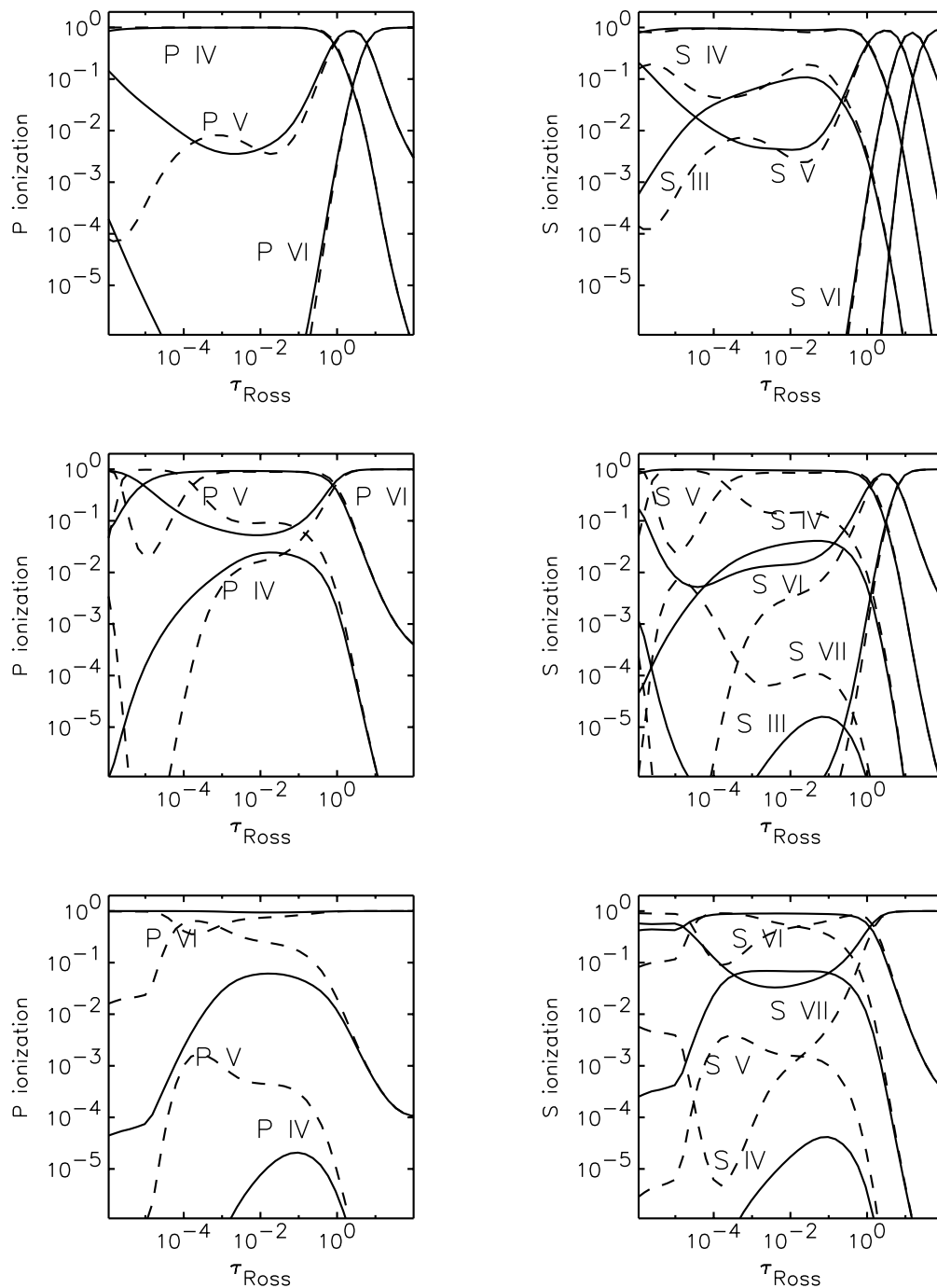
Fig. 8.—Same as Fig. 5, except for phosphorus and sulfur

This exercise shows that using Kurucz models is still a reasonable choice for analyzing *low-resolution* UV and optical spectra of O stars. It should be realized, however, that the full strength of NLTE models lies in their ability to provide reliable high-resolution spectra and profiles of individual lines that can be used for determining the stellar parameters and the surface chemical composition. We will study various systematic effects and differences between LTE and NLTE models, as well as their influence on deduced stellar parameters, in a future paper.

7. BOLOMETRIC CORRECTIONS AND IONIZING FLUXES

7.1. *Bolometric Corrections*

Bolometric corrections (Table 3) are calculated using the following expression:

$$\mathrm{BC} = m_{\mathrm{bol}} - V$$
$$= (-2.5 \log F_{\mathrm{bol}} - 11.487) - (-2.5 \log F_V - 21.100) ,$$
$$(1)$$
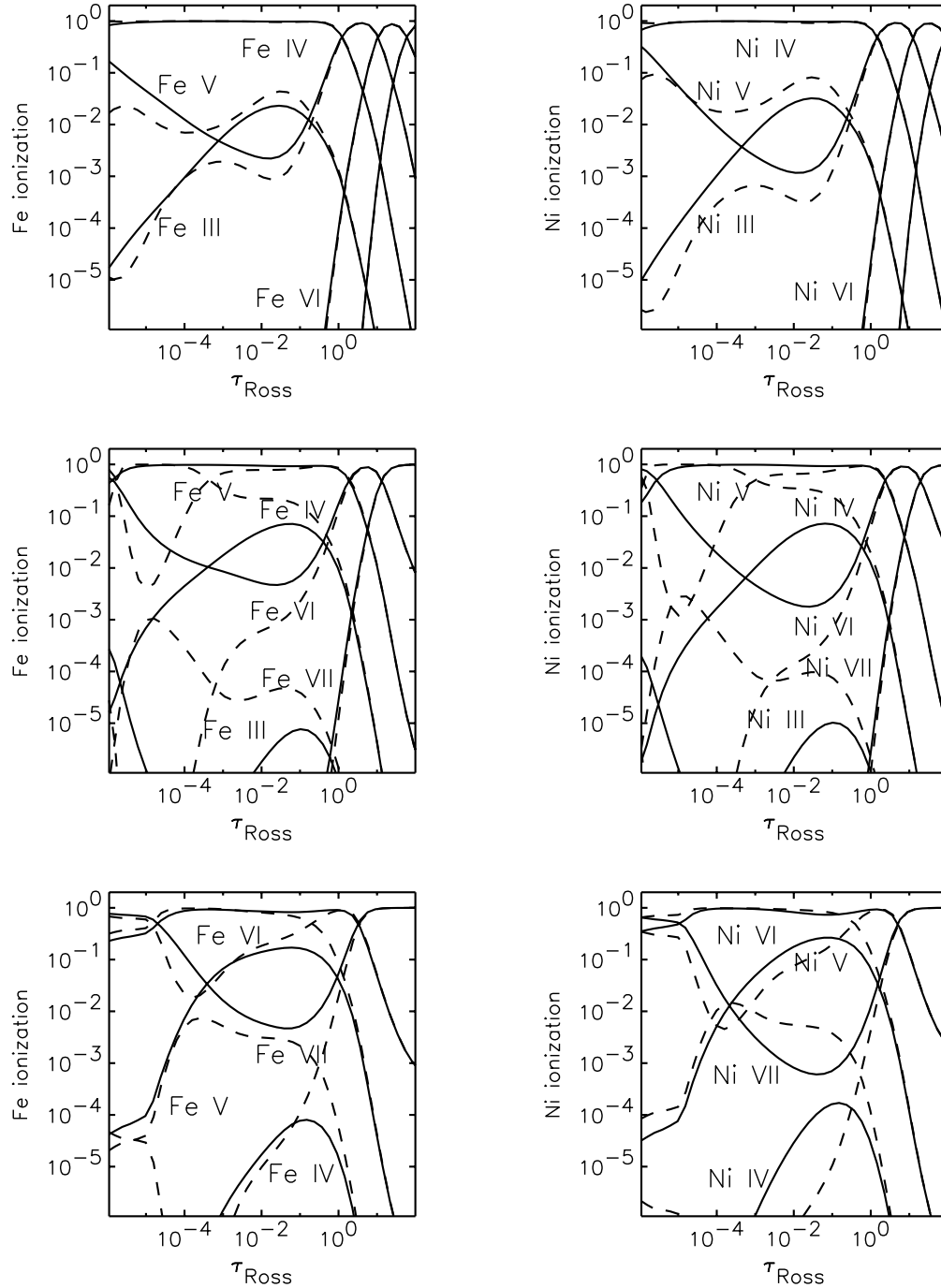
FIG. 9.—Same as Fig. 5, except for iron and nickel

where $F_{\rm bol}$ is the bolometric flux and F_V is the flux through the Johnson V filter, computed from the model atmospheres' flux distribution. The bolometric flux is computed by trapezoidal integration over the complete frequency range, while we have used an IDL version of the program UBVBUSER (Kurucz 1993) kindly made available by W. Landsman to obtain the V magnitudes. The first constant is defined by assuming a solar constant, $f_{\rm bol}^{\odot} = 1.371 \times 10^6$ ergs s^{-1} cm^{-2}, a solar visual magnitude, $V_{\odot} = -26.76$, and a solar bolometric correction, BC$_{\odot} = -0.07$, while the second constant defines the zero point of the V magnitude scale (Bessel, Castelli, & Plez 1998).

Figure 14 illustrates the major dependence of the bolometric correction on the effective temperature. Over the parameter space of the grid, a multilinear regression yields the relation

$$\mathrm{BC} = 27.43 - 6.78 \log T_{\rm eff} + 0.06 \frac{Z}{Z_{\odot}} \ . \qquad (2)$$

An inspection of Table 3 shows that the dependence with gravity is generally even smaller than the metallicity term. We have therefore neglected the gravity dependence, and equation (2) has been established with values from

FIG. 10.—Predicted flux for model atmospheres for $\log g = 4.0$, solar composition, and various effective temperatures: from top to bottom, $T_{\rm eff} = 55,000, 50,000, 45,000, 40,000, 35,000,$ and $30,000$ K.

FIG. 11.—Predicted flux for model atmospheres for $T_{\rm eff} = 40,000$ K, solar composition, and various surface gravities: from top to bottom at the Balmer continuum ($\lambda > 912$ Å), $\log g = 4.5, 4.25, 4.0, 3.75,$ and 3.5; the lowest gravity model is drawn by a thick line. Notice that the dependence of flux on $\log g$ is reversed in the Lyman continuum ($\lambda < 912$ Å).

$\log g = 4.0$ models. The typical accuracy of bolometric corrections derived from equation (2) is ± 0.05 mag. Larger differences up to 0.1 mag between the models and equation (2) values are found for the coolest models.

We compare our bolometric corrections to values calculated for Kurucz (1993) models and extracted from Bessel et al. (1998). We 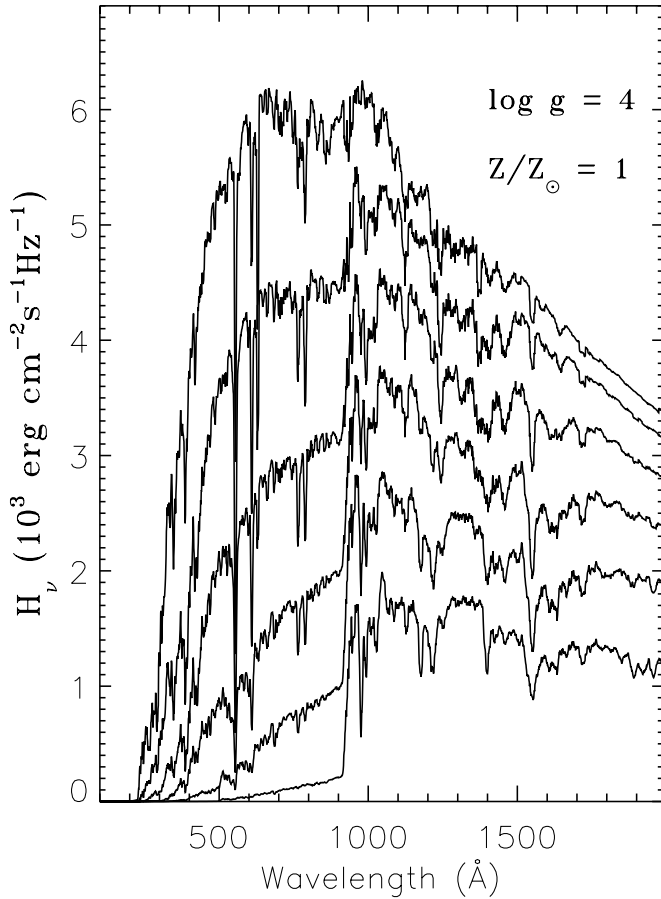use the same zero point for bolometric corrections. We find almost identical values for solar composition models with $\log g = 4.0$ and 4.5. The largest differences reach 0.03 mag at $T_{\rm eff} = 47,500$ K and 0.05 mag at $T_{\rm eff} = 27,500$ K, adding thus to the good agreement found in the previous section between SEDs (Fig. 13).

Our relation (eq. [2]) is close to the Vacca, Garmany, & Shull (1996) calibration, which is based on a number of diverse NLTE analyses. Their bolometric corrections are systematically smaller by 0.12 mag. Our relation therefore yields stellar luminosities 12% fainter than previously estimated from Vacca et al. (1996).

7.2. Ionizing Fluxes

We have calculated the ionizing fluxes in the hydrogen Lyman and in the He I $\lambda 504$ continua. They are listed in Tables 4 and 5. The ionizing fluxes, q_0 and q_1, are given as logarithms of the number of photons in these two continua, per second and per square centimeter at the stellar surface. We do not provide the ionizing flux q_2 in the He II Lyman continuum. Gabler, Kudritzki, & Mendez (1991) indeed

showed that the He II continuum is formed in a stellar wind (as a result of high opacity in this continuum) and that spherical extension and shocks are necessary model ingredients to predict fluxes that are in rough agreement with observed fluxes. However, the contribution of the He II Lyman continuum to q_0 and q_1 remains very small. Any error in q_2 results therefore in insignificant changes of q_0 and q_1. The latter fluxes are mostly sensitive to a correct treatment of NLTE metal line blanketing, which in turn is crucial to predict the hydrogen and helium ionization structure and the photospheric temperature stratification reliably.

The dependence of the ionization fluxes on $T_{\rm eff}$, $\log g$, and $Z/Z_\odot$ is displayed in Figure 15. Lower gravity models have larger ionizing fluxes as a result of higher hydrogen and helium ionization (thus the Lyman and $\lambda 504$ jumps are smaller). Model atmospheres with low metallicity have lower Lyman continuum fluxes. The behavior of the He I continuum fluxes is more complicated: at low $T_{\rm eff}$, metal-poor model atmospheres have markedly lower q_1 fluxes, while at $T_{\rm eff}$ higher than about 33,000 K, they have slightly larger q_1 fluxes. Lower metal abundances reduce the blanketing effect and thus result in lower temperatures in the continuum-forming layers and lower fluxes. The higher q_1 fluxes in hot, metal-poor models come from smaller metal line opacities in this spectral range.
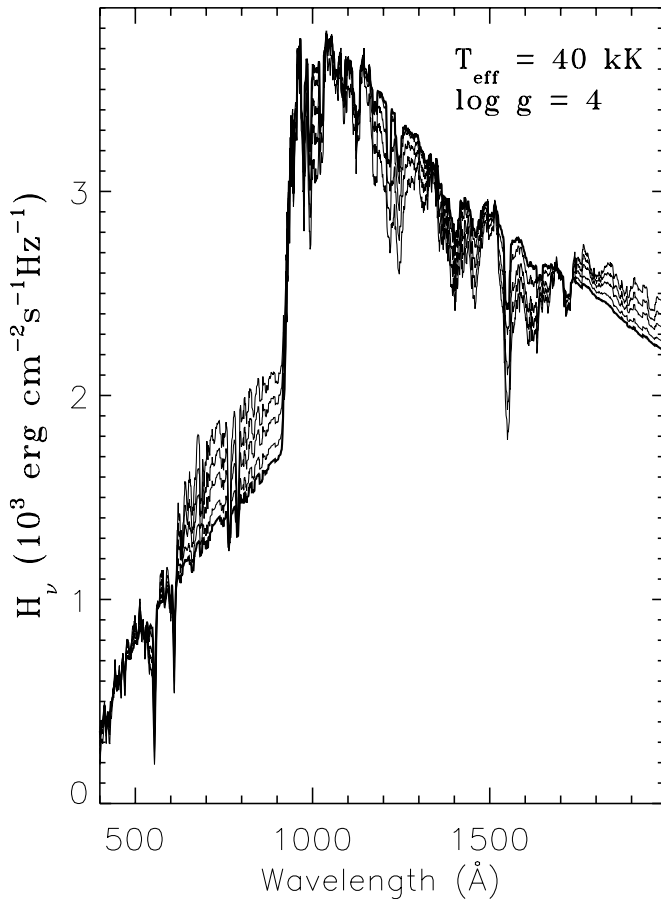
Fig. 12.—Predicted flux for model atmospheres for $T_{eff} = 40,000$ K, $\log g = 4.0$, and various metallicities: $Z/Z_\odot = 2$, 1, $\frac{1}{2}$, $\frac{1}{5}$, and 1/10. The flux for the lowest metallicity model is drawn by a thick line. The flux generally decreases with decreasing metallicity for $\lambda < 900$ Å and $\lambda > 1700$ Å, while the relation is reversed for 900 Å $< \lambda <$ 1700 Å.

We have compared our ionizing fluxes to other recent works. Vacca et al. (1996) used Kurucz (1993) LTE model fluxes to compute q_0 and q_1. They list 43 values for parameters covering the domain of O stars. We interpolate bilinearly in $\log T_{eff}$ and $\log g$ in Tables 4 and 5 and compare the Vacca et al. (1996) values. The q_0 values agree very well, with no systematic differences; we still found differences up to 0.1–0.2 dex for some parameters (mostly the coolest models). On the other hand, the q_1 values of Vacca et al. (1996) are on average 0.25 dex smaller than ours; individual differences range typically from 0.1 to 0.5 dex, increasing toward cooler effective temperatures. These differences are quite significant for nebular studies.

We have also compared our results to values derived from NLTE, line-blanketed, expanding model atmospheres, calculated with program WM-BASIC (Pauldrach et al. 2001). The q_0 values agree also very well, although our values are slightly larger. The values agree within 0.1 dex, with the exception of the two models, D-30 and S-30, at $T_{eff} = 30,000$ K, where WM-BASIC models predict ionizing fluxes smaller by 0.57 and 0.24 dex, respectively.

8. MODEL SENSITIVITY TO ATOMIC MODEL ATOMS

We have aimed at incorporating all important opacity sources and all relevant atomic processes that determine the excitation and ionization balance in the model atmospheres. To investigate the sensitivity of the model atmospheres to our handling of atomic data, we present here a few test cases in which we adopted different model atoms. We consider here two potential issues: (1) the size of the iron model atoms and the representation of the line opacity, and (2) the omission of highly excited levels in light elements (mostly CNO).

Kurucz (1994) lists thousands of energy levels for every iron ion. How should we group them? Our model atoms group them into 30–50 superlevels per ion. On the other hand, Deetjen et al. (1999) have grouped all individual levels into seven to nine NLTE superlevels for each iron ion. We have compared the effect of different Fe model data on the resulting model atmospheres with a test case, $T_{eff} = 35,000$ K, $\log g = 4.0$, solar composition, and $\xi_t = 10$ km s^{-1}. The reference model is extracted from the OSTAR2002 grid. The first three models deal with the representation of line opacity: OS with larger frequency step, ODF, and line strength selection (Fe and Ni lines are dynamically selected depending on a strength criterion; see § 4.10). In the case of the ODF model (Gb), all the Fe and Ni lines are used to set up the ODFs. In the second set of models, we have built different Fe IV and Fe V model atoms (they are the dominant ions; see Fig. 9). All individual levels are included in models Gd and Ge, but grouped in more (74 and 69 vs. 43 and 42) or less (33 and 19) superlevels. In the last model, all the Fe and Ni levels above the ionization limits are omitted. Table 6 summarizes the properties of the different models.

Figure 16 illustrates the changes in the model temperature atmosphere structure due to different ways of including the iron data. This is a condensed way to assess differences between model atmospheres. We may indeed expect that model spectra change with changes in the temperature structure (this does not exclude of course that some line profiles might be different even with very close temperature structures; see below). First, differences are larger with ODFs than when adopting a rather large sampling step. We interpret this as reflecting incorrect blends between ODFs and important lines of light elements. The larger sampling step is probably appropriate in many cases ($\Delta T \approx 100$ K) and reduces the computing time by a factor of about 3 (the reduction in the number of frequency points). The largest difference arising as a result of the line strength selection criterion is seen at depth because of a large change in the number of selected Fe VI lines. However, this does not affect the predicted spectrum. Differences in the layers where the spectrum is formed are small ($\Delta T < 100$ K), showing that most of the line-blanketing effect is due to the strongest 10^4–10^5 lines rather than to millions of weaker lines. The bottom panels of Figure 16 show the results related to the model atoms. First, we see that increasing the number of superlevels results in small changes, while the model with less superlevels shows a larger systematic temperature difference. Although limited in scope (one set of stellar parameters), this test thus supports a claim that we have adopted Fe model atoms of reasonable sizes for our grid of model atmospheres. Finally, the levels above the ionization limits have a minimal effect on the model atmosphere structure.

In a second test, we have investigated the omission of highly excited levels of light elements. Section 4 details the adopted model atoms. In some cases, levels with main quantum number, $n \geq 7$, have been neglected (e.g., C III and N IV). We have built a new C III model atom, which includes
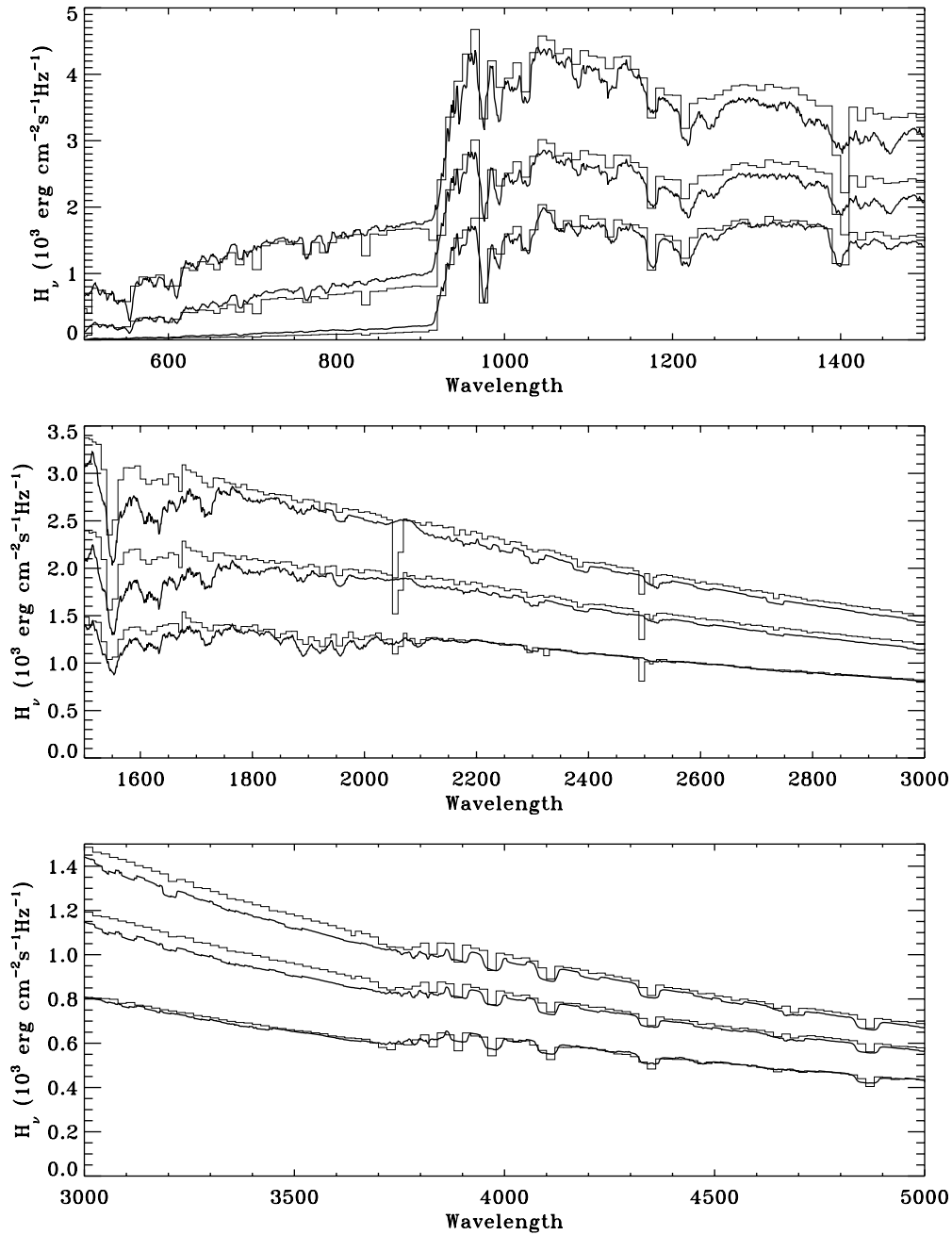
FIG. 13.—Predicted flux for three model atmospheres with (T_{eff}, $\log g$) equal to (40,000 K, 4.5), (35,000 K, 4.0), and (30,000 K, 4.0) (*thick lines*), compared to Kurucz models with the same parameters (*thin histograms*). Different panels show different spectrum regions.

all levels below the ionization limit that are considered in OP calculations. The new model atom includes the first 34 levels as individual explicit levels and groups higher levels into 12 superlevels. We have recomputed one model atmosphere, S35000g325v10, assuming the extended C III model atom. The atmospheric structure is changed very little ($\Delta T < 8$ K), and this omission is therefore mostly of no consequence.

However, the total recombination rate, from C^{+3} to C^{+2}, is significantly increased, by a factor of 2–3. Recombination lines in the optical, e.g., C III $\lambda 4650$, show thus significantly stronger emission in the new model. We note here in passing that these "Of-type" lines are predicted in emission by plane-parallel, hydrostatic, NLTE model atmospheres at

low gravities (Mihalas & Hummer 1973). These are NLTE recombination lines, and emission is neither a consequence of a stellar wind nor of an extended atmosphere. We caution therefore against using the current grid for quantitative analysis of weak absorption or emission features in the optical spectrum without a careful investigation case by case. A future update is expected.

9. DISCUSSION AND CONCLUSIONS

We have constructed a comprehensive grid of metal line–blanketed, NLTE, plane-parallel, hydrostatic model atmospheres for the basic parameters appropriate to O-type stars. The OSTAR2002 grid considers 12 values of effective

TABLE 3

Bolometric Corrections as a Function of Effective Temperature, Gravity, and Metallicity (10 Metallicities from 2 Times Solar to Metal-free Models)

$T_{\rm eff}$ (K)	log g	BC (mag) 2.	1.	0.5	0.2	0.1	0.033	0.02	0.01	0.001	0.
27,500	3.00	−2.59	−2.62	−2.65	−2.68	−2.71	−2.73	−2.74	−2.75	−2.76	−2.76
	3.25	−2.56	−2.61	−2.65	−2.69	−2.71	−2.73	−2.74	−2.74	−2.75	−2.75
	3.50	−2.57	−2.62	−2.66	−2.70	−2.72	−2.74	−2.75	−2.76	−2.76	−2.76
	3.75	−2.59	−2.64	−2.68	−2.72	−2.74	−2.76	−2.77	−2.77	−2.78	−2.78
	4.00	−2.60	−2.65	−2.69	−2.73	−2.75	−2.77	−2.78	−2.78	−2.79	−2.80
	4.25	−2.62	−2.67	−2.71	−2.74	−2.76	−2.78	−2.79	−2.79	−2.80	−2.81
	4.50	−2.63	−2.68	−2.72	−2.75	−2.77	−2.79	−2.80	−2.80	−2.81	−2.81
	4.75	−2.64	−2.69	−2.72	−2.76	−2.78	−2.80	−2.80	−2.81	−2.82	−2.82
30,000	3.00	−2.92	−2.92	−2.92	−2.94	−2.95	−2.97	−2.98	−2.99	−3.00	−3.00
	3.25	−2.80	−2.83	−2.86	−2.89	−2.91	−2.93	−2.94	−2.95	−2.96	−2.96
	3.50	−2.78	−2.82	−2.86	−2.90	−2.92	−2.94	−2.94	−2.95	−2.96	−2.96
	3.75	−2.79	−2.84	−2.88	−2.91	−2.93	−2.95	−2.95	−2.96	−2.96	−2.97
	4.00	−2.81	−2.85	−2.89	−2.93	−2.94	−2.96	−2.97	−2.97	−2.98	−2.98
	4.25	−2.82	−2.87	−2.90	−2.94	−2.96	−2.97	−2.98	−2.98	−2.99	−2.99
	4.50	−2.84	−2.88	−2.92	−2.95	−2.97	−2.98	−2.99	−2.99	−3.00	−3.00
	4.75	−2.85	−2.89	−2.93	−2.96	−2.97	−2.99	−3.00	−3.00	−3.01	−3.01
32,500	3.25	−3.07	−3.08	−3.10	−3.12	−3.14	−3.16	−3.16	−3.17	−3.18	−3.18
	3.50	−3.01	−3.04	−3.06	−3.09	−3.11	−3.13	−3.14	−3.14	−3.15	−3.15
	3.75	−3.00	−3.03	−3.06	−3.09	−3.11	−3.13	−3.13	−3.14	−3.15	−3.15
	4.00	−3.00	−3.04	−3.07	−3.10	−3.12	−3.14	−3.14	−3.14	−3.15	−3.15
	4.25	−3.01	−3.05	−3.08	−3.11	−3.13	−3.14	−3.15	−3.15	−3.16	−3.16
	4.50	−3.03	−3.06	−3.10	−3.12	−3.14	−3.15	−3.15	−3.16	−3.16	−3.16
	4.75	−3.04	−3.08	−3.11	−3.13	−3.15	−3.16	−3.16	−3.16	−3.17	−3.17
35,000	3.25	−3.35	−3.36	−3.37	−3.38	−3.39	−3.40	−3.41	−3.41	−3.42	−3.42
	3.50	−3.25	−3.27	−3.29	−3.32	−3.33	−3.35	−3.35	−3.35	−3.36	−3.36
	3.75	−3.22	−3.24	−3.27	−3.29	−3.31	−3.33	−3.33	−3.33	−3.34	−3.34
	4.00	−3.21	−3.24	−3.26	−3.29	−3.30	−3.32	−3.32	−3.33	−3.33	−3.33
	4.25	−3.21	−3.24	−3.26	−3.29	−3.30	−3.32	−3.32	−3.32	−3.33	−3.33
	4.50	−3.21	−3.24	−3.27	−3.30	−3.31	−3.32	−3.32	−3.33	−3.33	−3.33
	4.75	−3.22	−3.25	−3.28	−3.30	−3.31	−3.32	−3.32	−3.33	−3.33	−3.33
37,500	3.50	−3.48	−3.50	−3.52	−3.54	−3.55	−3.57	−3.57	−3.58	−3.58	−3.58
	3.75	−3.44	−3.46	−3.48	−3.51	−3.52	−3.53	−3.54	−3.54	−3.54	−3.55
	4.00	−3.42	−3.45	−3.47	−3.49	−3.50	−3.52	−3.52	−3.52	−3.53	−3.53
	4.25	−3.41	−3.44	−3.46	−3.48	−3.50	−3.51	−3.51	−3.51	−3.52	−3.52
	4.50	−3.41	−3.43	−3.46	−3.48	−3.49	−3.50	−3.51	−3.51	−3.51	−3.51
	4.75	−3.41	−3.44	−3.46	−3.48	−3.49	−3.50	−3.50	−3.51	−3.51	−3.51
40,000	3.50	−3.72	−3.73	−3.74	−3.76	−3.77	−3.78	−3.79	−3.79	−3.80	−3.80
	3.75	−3.64	−3.67	−3.69	−3.71	−3.73	−3.74	−3.74	−3.75	−3.75	−3.75
	4.00	−3.62	−3.65	−3.67	−3.69	−3.71	−3.72	−3.72	−3.72	−3.73	−3.73
	4.25	−3.61	−3.64	−3.66	−3.68	−3.69	−3.71	−3.71	−3.71	−3.71	−3.71
	4.50	−3.61	−3.63	−3.65	−3.67	−3.69	−3.70	−3.70	−3.70	−3.70	−3.71
	4.75	−3.60	−3.63	−3.65	−3.67	−3.68	−3.69	−3.69	−3.70	−3.70	−3.70
42,500	3.75	−3.84	−3.86	−3.88	−3.91	−3.92	−3.93	−3.94	−3.94	−3.95	−3.95
	4.00	−3.81	−3.84	−3.86	−3.88	−3.90	−3.91	−3.91	−3.92	−3.92	−3.92
	4.25	−3.80	−3.83	−3.85	−3.87	−3.89	−3.90	−3.90	−3.90	−3.91	−3.91
	4.50	−3.80	−3.82	−3.84	−3.87	−3.88	−3.89	−3.89	−3.89	−3.90	−3.90
	4.75	−3.80	−3.82	−3.84	−3.86	−3.87	−3.88	−3.88	−3.89	−3.89	−3.89
45,000	3.75	−4.05	−4.06	−4.08	−4.10	−4.11	−4.12	−4.13	−4.13	−4.14	−4.14
	4.00	−3.99	−4.02	−4.04	−4.06	−4.08	−4.09	−4.10	−4.10	−4.11	−4.11
	4.25	−3.98	−4.01	−4.03	−4.05	−4.07	−4.08	−4.08	−4.09	−4.09	−4.09
	4.50	−3.98	−4.00	−4.02	−4.05	−4.06	−4.07	−4.07	−4.08	−4.08	−4.08
	4.75	−3.98	−4.00	−4.02	−4.04	−4.05	−4.07	−4.07	−4.07	−4.08	−4.08
47,500	4.00	−4.17	−4.20	−4.22	−4.24	−4.25	−4.26	−4.27	−4.27	−4.28	−4.29
	4.25	−4.15	−4.18	−4.20	−4.22	−4.24	−4.25	−4.25	−4.26	−4.27	−4.27
	4.50	−4.15	−4.17	−4.19	−4.22	−4.23	−4.24	−4.25	−4.25	−4.26	−4.26
	4.75	−4.14	−4.17	−4.19	−4.21	−4.23	−4.24	−4.24	−4.25	−4.25	−4.25
50,000	4.00	−4.35	−4.37	−4.39	−4.41	−4.42	−4.43	−4.44	−4.44	−4.45	−4.45
	4.25	−4.32	−4.34	−4.36	−4.39	−4.40	−4.41	−4.42	−4.42	−4.43	−4.43
	4.50	−4.31	−4.33	−4.36	−4.38	−4.39	−4.41	−4.41	−4.41	−4.42	−4.42
	4.75	−4.30	−4.33	−4.35	−4.38	−4.39	−4.40	−4.41	−4.41	−4.42	−4.42

434

TABLE 3—*Continued*

$T_{\rm eff}$ (K)	$\log g$	BC (mag)									
		2.	1.	0.5	0.2	0.1	0.033	0.02	0.01	0.001	0.
52,500	4.00	−4.52	−4.54	−4.55	−4.57	−4.58	−4.60	−4.60	−4.60	−4.61	−4.61
	4.25	−4.48	−4.50	−4.52	−4.54	−4.56	−4.57	−4.58	−4.58	−4.59	−4.59
	4.50	−4.46	−4.49	−4.51	−4.53	−4.55	−4.56	−4.57	−4.57	−4.58	−4.58
	4.75	−4.46	−4.49	−4.51	−4.53	−4.54	−4.56	−4.56	−4.57	−4.57	−4.58
55,000	4.00	−4.69	−4.71	−4.72	−4.74	−4.75	−4.76	−4.76	−4.76	−4.77	−4.77
	4.25	−4.63	−4.66	−4.68	−4.70	−4.71	−4.72	−4.73	−4.73	−4.74	−4.74
	4.50	−4.62	−4.64	−4.66	−4.69	−4.70	−4.71	−4.72	−4.72	−4.73	−4.73
	4.75	−4.61	−4.64	−4.66	−4.68	−4.69	−4.71	−4.71	−4.72	−4.72	−4.73

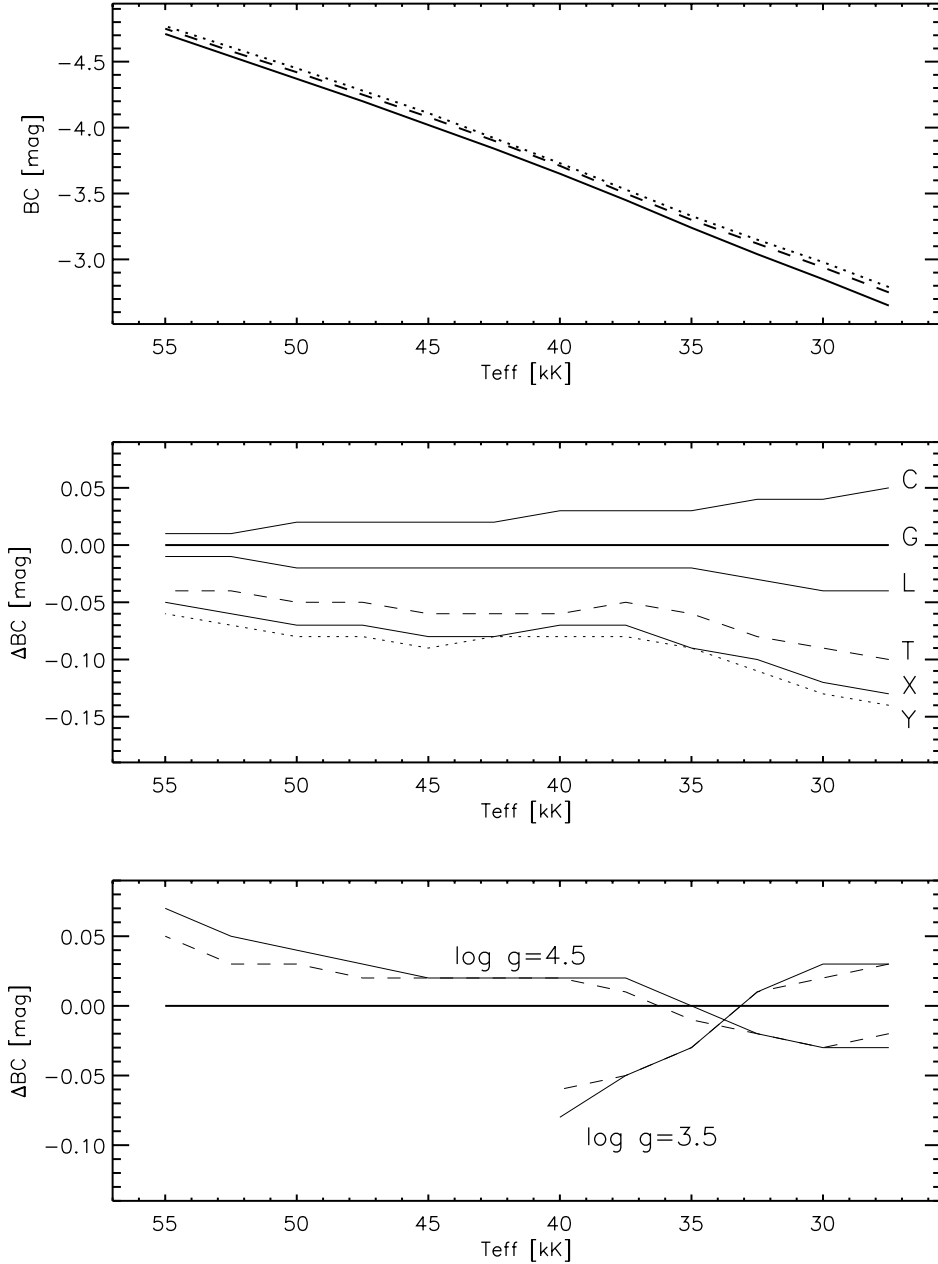
FIG. 14.—Bolometric corrections vs. effective temperature. *Top:* Relation for $\log g = 4.0$, solar composition (*solid line*), 1/10 (*dashed line*), and 1/1000 solar (*dotted line*). *Middle:* Expansion on the effect of metallicity on BC, displaying differences relative to solar models ($\log g = 4.0$). *Bottom:* Effect of different gravities (*solid line:* solar; *dashed line:* 1/10 solar).

TABLE 4
Ionizing Fluxes in the H i Lyman Continuum as a Function of Effective Temperature, Gravity, and Metallicity (10 Metallicities from 2 Times Solar to Metal-free Models)

$T_{\rm eff}$ (K)	$\log g$	2.	1.	0.5	0.2	0.1	0.033	0.02	0.01	0.001	0.
		$q_0 = \log N_{\rm Lyc}$ (s^{-1} cm^{-2})									
27,500	3.00	23.26	23.21	23.18	23.15	23.14	23.13	23.13	23.13	23.14	23.15
	3.25	23.00	22.93	22.87	22.81	22.78	22.76	22.75	22.74	22.74	22.75
	3.50	22.79	22.70	22.62	22.53	22.48	22.41	22.39	22.37	22.33	22.33
	3.75	22.62	22.52	22.43	22.33	22.26	22.17	22.14	22.10	22.03	22.01
	4.00	22.49	22.39	22.30	22.19	22.12	22.01	21.97	21.93	21.84	21.82
	4.25	22.39	22.28	22.19	22.08	22.01	21.90	21.86	21.81	21.73	21.70
	4.50	22.30	22.20	22.11	22.00	21.92	21.82	21.78	21.74	21.66	21.64
	4.75	22.23	22.13	22.03	21.92	21.85	21.76	21.72	21.68	21.61	21.59
30,000	3.00	23.68	23.66	23.65	23.64	23.63	23.63	23.63	23.63	23.63	23.63
	3.25	23.51	23.47	23.44	23.42	23.41	23.40	23.40	23.40	23.41	23.41
	3.50	23.36	23.30	23.26	23.21	23.19	23.18	23.17	23.17	23.18	23.18
	3.75	23.22	23.15	23.08	23.02	22.99	22.96	22.95	22.95	22.94	22.95
	4.00	23.10	23.01	22.94	22.86	22.81	22.76	22.75	22.74	22.73	22.73
	4.25	22.99	22.89	22.81	22.72	22.67	22.61	22.59	22.58	22.56	22.55
	4.50	22.90	22.80	22.71	22.62	22.56	22.50	22.48	22.46	22.43	22.43
	4.75	22.82	22.72	22.63	22.54	22.49	22.42	22.40	22.38	22.34	22.34
32,500	3.25	23.84	23.82	23.81	23.79	23.79	23.78	23.78	23.78	23.78	23.78
	3.50	23.73	23.70	23.68	23.66	23.65	23.64	23.64	23.64	23.64	23.64
	3.75	23.64	23.60	23.56	23.53	23.52	23.51	23.51	23.51	23.51	23.51
	4.00	23.55	23.50	23.45	23.41	23.39	23.38	23.38	23.38	23.38	23.38
	4.25	23.47	23.41	23.36	23.31	23.28	23.26	23.26	23.26	23.26	23.26
	4.50	23.40	23.33	23.27	23.21	23.21	23.16	23.15	23.15	23.15	23.15
	4.75	23.34	23.26	23.20	23.13	23.10	23.07	23.07	23.06	23.06	23.06
35,000	3.25	24.09	24.08	24.07	24.06	24.06	24.05	24.05	24.05	24.05	24.05
	3.50	23.99	23.98	23.97	23.95	23.95	23.94	23.94	23.94	23.94	23.94
	3.75	23.92	23.90	23.88	23.87	23.86	23.85	23.85	23.85	23.85	23.85
	4.00	23.87	23.84	23.81	23.79	23.78	23.77	23.77	23.77	23.77	23.77
	4.25	23.81	23.78	23.75	23.72	23.71	23.70	23.70	23.70	23.70	23.70
	4.50	23.77	23.72	23.69	23.66	23.64	23.64	23.64	23.64	23.64	23.64
	4.75	23.72	23.67	23.64	23.60	23.59	23.58	23.58	23.58	23.58	23.58
37,500	3.50	24.21	24.20	24.19	24.18	24.17	24.17	24.17	24.16	24.16	24.16
	3.75	24.14	24.13	24.12	24.11	24.10	24.10	24.09	24.09	24.09	24.09
	4.00	24.10	24.08	24.07	24.05	24.04	24.04	24.04	24.04	24.04	24.04
	4.25	24.06	24.04	24.02	24.00	24.00	23.99	23.99	23.99	23.99	23.99
	4.50	24.03	24.00	23.98	23.96	23.96	23.95	23.95	23.95	23.95	23.95
	4.75	24.00	23.97	23.95	23.93	23.92	23.92	23.91	23.91	23.92	23.92
40,000	3.50	24.39	24.38	24.37	24.36	24.36	24.35	24.35	24.35	24.34	24.34
	3.75	24.33	24.32	24.31	24.30	24.30	24.29	24.29	24.28	24.28	24.28
	4.00	24.29	24.28	24.27	24.26	24.25	24.24	24.24	24.24	24.24	24.24
	4.25	24.26	24.24	24.23	24.22	24.21	24.20	24.20	24.20	24.20	24.20
	4.50	24.23	24.21	24.20	24.19	24.18	24.18	24.17	24.17	24.17	24.17
	4.75	24.21	24.19	24.18	24.16	24.16	24.15	24.15	24.15	24.15	24.15
42,500	3.75	24.49	24.48	24.47	24.46	24.46	24.45	24.45	24.45	24.44	24.44
	4.00	24.45	24.44	24.43	24.42	24.42	24.41	24.41	24.40	24.40	24.40
	4.25	24.43	24.41	24.40	24.39	24.38	24.38	24.38	24.37	24.37	24.37
	4.50	24.40	24.39	24.38	24.37	24.36	24.35	24.35	24.35	24.35	24.35
	4.75	24.39	24.37	24.36	24.35	24.34	24.34	24.33	24.33	24.33	24.33
45,000	3.75	24.62	24.62	24.61	24.60	24.60	24.59	24.59	24.59	24.58	24.58
	4.00	24.59	24.58	24.58	24.57	24.56	24.55	24.55	24.55	24.55	24.54
	4.25	24.57	24.56	24.55	24.54	24.53	24.53	24.52	24.52	24.52	24.52
	4.50	24.55	24.54	24.53	24.52	24.51	24.50	24.50	24.50	24.50	24.50
	4.75	24.54	24.52	24.51	24.50	24.50	24.49	24.49	24.48	24.48	24.48
47,500	4.00	24.72	24.71	24.70	24.69	24.69	24.68	24.68	24.68	24.67	24.67
	4.25	24.70	24.69	24.68	24.67	24.66	24.65	24.65	24.65	24.65	24.65
	4.50	24.68	24.67	24.66	24.65	24.64	24.64	24.63	24.63	24.63	24.63
	4.75	24.67	24.66	24.65	24.64	24.63	24.62	24.62	24.62	24.61	24.61
50,000	4.00	24.82	24.82	24.81	24.80	24.80	24.79	24.79	24.79	24.79	24.78
	4.25	24.81	24.80	24.79	24.78	24.78	24.77	24.77	24.77	24.76	24.76
	4.50	24.80	24.79	24.78	24.77	24.76	24.75	24.75	24.75	24.74	24.74
	4.75	24.79	24.78	24.76	24.75	24.75	24.74	24.74	24.74	24.73	24.73

TABLE 4—*Continued*

T_{eff} (K)	$\log g$	$q_0 = \log N_{Lyc}$ $(s^{-1}\ cm^{-2})$									
		2.	1.	0.5	0.2	0.1	0.033	0.02	0.01	0.001	0.
52,500	4.00	24.92	24.92	24.91	24.90	24.90	24.90	24.89	24.89	24.89	24.89
	4.25	24.91	24.90	24.89	24.89	24.88	24.87	24.87	24.87	24.87	24.87
	4.50	24.90	24.89	24.88	24.87	24.87	24.86	24.86	24.85	24.85	24.85
	4.75	24.89	24.88	24.87	24.86	24.85	24.85	24.84	24.84	24.84	24.84
55,000	4.00	25.01	25.01	25.00	25.00	24.99	24.99	24.99	24.99	24.98	24.98
	4.25	25.00	24.99	24.99	24.98	24.98	24.97	24.97	24.97	24.96	24.96
	4.50	24.99	24.98	24.97	24.97	24.96	24.96	24.95	24.95	24.95	24.95
	4.75	24.98	24.97	24.97	24.96	24.95	24.94	24.94	24.94	24.94	24.94

TABLE 5

IONIZING FLUXES IN THE He I CONTINUUM AS A FUNCTION OF EFFECTIVE TEMPERATURE, GRAVITY,
AND METALLICITY (10 METALLICITIES FROM 2 TIMES SOLAR TO METAL-FREE MODELS)

T_{eff} (K)	$\log g$	$q_1 = \log N_{504}$ $(s^{-1}\ cm^{-2})$									
		2.	1.	0.5	0.2	0.1	0.033	0.02	0.01	0.001	0.
27,500	3.00	20.85	20.80	20.74	20.69	20.65	20.61	20.60	20.58	20.55	20.53
	3.25	20.45	20.35	20.25	20.10	19.99	19.82	19.76	19.71	19.62	19.60
	3.50	20.17	20.03	19.89	19.68	19.52	19.30	19.21	19.13	19.00	18.98
	3.75	19.95	19.80	19.64	19.40	19.22	18.95	18.86	18.76	18.60	18.57
	4.00	19.79	19.63	19.45	19.20	19.01	18.73	18.63	18.53	18.37	18.34
	4.25	19.66	19.49	19.31	19.05	18.85	18.58	18.48	18.39	18.24	18.21
	4.50	19.55	19.37	19.18	18.92	18.72	18.46	18.37	18.29	18.16	18.13
	4.75	19.45	19.26	19.07	18.80	18.61	18.37	18.29	18.22	18.11	18.08
30,000	3.00	22.29	22.31	22.33	22.35	22.38	22.41	22.43	22.45	22.47	22.48
	3.25	21.55	21.51	21.50	21.52	21.56	21.61	21.63	21.66	21.70	21.70
	3.50	21.12	21.06	21.00	20.94	20.89	20.84	20.82	20.81	20.78	20.77
	3.75	20.90	20.81	20.71	20.58	20.49	20.36	20.32	20.28	20.22	20.21
	4.00	20.73	20.61	20.48	20.31	20.18	20.02	19.97	19.92	19.85	19.83
	4.25	20.59	20.45	20.30	20.10	19.96	19.77	19.71	19.66	19.58	19.56
	4.50	20.46	20.31	20.15	19.94	19.79	19.60	19.54	19.47	19.39	19.37
	4.75	20.36	20.20	20.04	19.82	19.67	19.47	19.41	19.35	19.27	19.25
32,500	3.25	22.61	22.64	22.67	22.70	22.73	22.77	22.78	22.80	22.82	22.83
	3.50	22.24	22.25	22.27	22.30	22.34	22.39	22.41	22.43	22.47	22.48
	3.75	21.87	21.85	21.85	21.87	21.90	21.95	21.97	21.99	22.04	22.05
	4.00	21.61	21.56	21.53	21.51	21.51	21.51	21.52	21.53	21.56	21.56
	4.25	21.44	21.38	21.32	21.25	21.21	21.17	21.16	21.15	21.15	21.14
	4.50	21.32	21.24	21.15	21.05	20.99	20.92	20.90	20.88	20.86	20.85
	4.75	21.22	21.12	21.02	20.90	20.82	20.73	20.71	20.69	20.66	20.65
35,000	3.25	23.12	23.15	23.17	23.21	23.23	23.26	23.27	23.28	23.30	23.31
	3.50	22.92	22.96	22.99	23.03	23.05	23.09	23.10	23.12	23.14	23.15
	3.75	22.75	22.77	22.80	22.83	22.86	22.91	22.93	22.95	22.98	22.98
	4.00	22.56	22.58	22.60	22.63	22.66	22.71	22.74	22.76	22.80	22.80
	4.25	22.38	22.38	22.40	22.43	22.46	22.51	22.54	22.56	22.60	22.61
	4.50	22.21	22.21	22.22	22.24	22.27	22.32	22.34	22.37	22.41	22.41
	4.75	22.08	22.07	22.06	22.08	22.10	22.13	22.15	22.18	22.22	22.22
37,500	3.50	23.30	23.34	23.37	23.41	23.43	23.46	23.47	23.48	23.50	23.51
	3.75	23.21	23.24	23.27	23.31	23.34	23.37	23.39	23.40	23.42	23.42
	4.00	23.12	23.15	23.18	23.21	23.24	23.28	23.30	23.31	23.34	23.34
	4.25	23.03	23.06	23.08	23.12	23.15	23.19	23.21	23.23	23.25	23.26
	4.50	22.94	22.97	22.99	23.03	23.05	23.10	23.12	23.14	23.17	23.17
	4.75	22.85	22.87	22.90	22.94	22.97	23.02	23.04	23.06	23.08	23.09
40,000	3.50	23.60	23.62	23.64	23.67	23.69	23.72	23.72	23.73	23.75	23.75
	3.75	23.51	23.54	23.57	23.61	23.63	23.66	23.67	23.68	23.70	23.70
	4.00	23.46	23.49	23.52	23.56	23.58	23.62	23.63	23.64	23.66	23.66
	4.25	23.41	23.44	23.47	23.51	23.54	23.57	23.59	23.60	23.61	23.62
	4.50	23.37	23.40	23.42	23.46	23.49	23.53	23.54	23.55	23.57	23.58
	4.75	23.32	23.35	23.38	23.42	23.44	23.49	23.50	23.51	23.53	23.53

TABLE 5—*Continued*

$T_{\rm eff}$ (K)	$\log g$	$q_1 = \log N_{504}$ (s^{-1} cm^{-2})									
		2.	1.	0.5	0.2	0.1	0.033	0.02	0.01	0.001	0.
42,500	3.75	23.75	23.77	23.80	23.83	23.85	23.87	23.88	23.89	23.91	23.91
	4.00	23.70	23.73	23.76	23.80	23.82	23.85	23.86	23.87	23.88	23.89
	4.25	23.67	23.71	23.74	23.77	23.80	23.83	23.84	23.85	23.86	23.87
	4.50	23.65	23.68	23.71	23.75	23.78	23.81	23.82	23.83	23.84	23.84
	4.75	23.63	23.66	23.69	23.73	23.75	23.79	23.80	23.81	23.82	23.82
45,000	3.75	23.96	23.98	24.00	24.03	24.04	24.06	24.06	24.07	24.08	24.08
	4.00	23.91	23.94	23.96	23.99	24.01	24.03	24.04	24.05	24.06	24.07
	4.25	23.88	23.91	23.94	23.98	24.00	24.02	24.03	24.04	24.05	24.05
	4.50	23.87	23.90	23.93	23.97	23.99	24.01	24.02	24.03	24.04	24.04
	4.75	23.86	23.89	23.92	23.95	23.98	24.00	24.01	24.02	24.03	24.03
47,500	4.00	24.09	24.12	24.14	24.16	24.18	24.19	24.20	24.21	24.22	24.22
	4.25	24.07	24.09	24.12	24.15	24.16	24.18	24.19	24.20	24.21	24.21
	4.50	24.05	24.08	24.11	24.14	24.16	24.18	24.19	24.19	24.20	24.21
	4.75	24.04	24.07	24.10	24.14	24.16	24.18	24.18	24.19	24.20	24.20
50,000	4.00	24.26	24.28	24.30	24.32	24.33	24.34	24.34	24.35	24.35	24.36
	4.25	24.23	24.26	24.28	24.30	24.31	24.33	24.33	24.34	24.35	24.35
	4.50	24.22	24.24	24.27	24.29	24.31	24.32	24.33	24.34	24.35	24.35
	4.75	24.21	24.24	24.26	24.29	24.31	24.32	24.33	24.34	24.35	24.35
52,500	4.00	24.42	24.43	24.44	24.46	24.46	24.47	24.47	24.47	24.48	24.48
	4.25	24.38	24.40	24.42	24.44	24.45	24.46	24.46	24.47	24.47	24.47
	4.50	24.37	24.39	24.41	24.43	24.44	24.45	24.46	24.46	24.47	24.47
	4.75	24.36	24.38	24.40	24.43	24.44	24.46	24.46	24.47	24.47	24.48
55,000	4.00	24.56	24.57	24.58	24.58	24.59	24.59	24.59	24.59	24.60	24.60
	4.25	24.52	24.54	24.55	24.56	24.57	24.58	24.58	24.58	24.59	24.59
	4.50	24.50	24.52	24.54	24.55	24.56	24.57	24.57	24.58	24.59	24.59
	4.75	24.49	24.52	24.53	24.55	24.56	24.57	24.58	24.58	24.59	24.59

temperatures, $27{,}500\text{ K} \le T_{\rm eff} \le 55{,}000\text{ K}$, with 2500 K steps, eight surface gravities, $3.0 \le \log g \le 4.75$, with 0.25 dex steps, and 10 chemical compositions, from metal-rich relative to the Sun to metal-free. The lower limit of $\log g$ for a given $T_{\rm eff}$ is actually set by an approximate location of the Eddington limit. The selected chemical compositions have been chosen to cover a number of typical environments of massive stars: the Galactic center, the Magellanic Clouds, blue compact dwarf galaxies like I Zw 18, and galaxies at high redshifts. The paper contains a description of the OSTAR2002 grid and some illustrative examples and comparisons. The complete OSTAR2002 grid is available on-line (see footnote 2).

We are aware that the presented grid cannot represent the last word in O star model stellar atmospheres. However, we intended to provide a more or less definitive grid of model atmospheres in the context of one-dimensional, plane-parallel, homogeneous, hydrostatic models in radiative equilibrium. We have attempted to take into account essen-

tially all important opacity sources (lines and continua) of all astrophysically important ions. Likewise, we have attempted to consider all relevant atomic processes that determine the excitation and ionization balance of all such atoms and ions. In other words, since the computational effort behind constructing the above described 680 models is enormous, we intended to compute as complete and realistic models as possible, in order to avoid the need to recompute a grid in the near future should some neglected mechanism or an opacity source be found to be important.

Although we spent all effort to make sure that the treatment of atomic physics and opacities is as complete and accurate as possible, there are still several points we are aware of that were crudely approximated. Those approximations were necessitated not by shortcomings of our modeling scheme or a lack of adequate computer resources, but by the present lack of sufficient atomic data. These approximations include the following (roughly in the order of estimated importance):

TABLE 6
ASSUMPTIONS AND CHARACTERISTICS FOR THE TEST CASE MODELS

| Model	Characteristics	Levels	Frequencies	Fe Lines
G35000g400v10	Reference model (OS, 0.75)	907	1,841,36	1,176,853
Ga35............................	OS, 30 Doppler widths	907	65,398	1,176,821
Gb35............................	ODF	907	40,759	7,459,416
Gc35	Fewer selected Fe/Ni lines	907	184,136	88,009
Gd35............................	More Fe IV–Fe V superlevels	965	65,493	1,221,466
Ge35	Less Fe IV–Fe V superlevels	874	65,366	952,051
Gf35............................	No levels above ionization limit	804	184,226	1,168,764
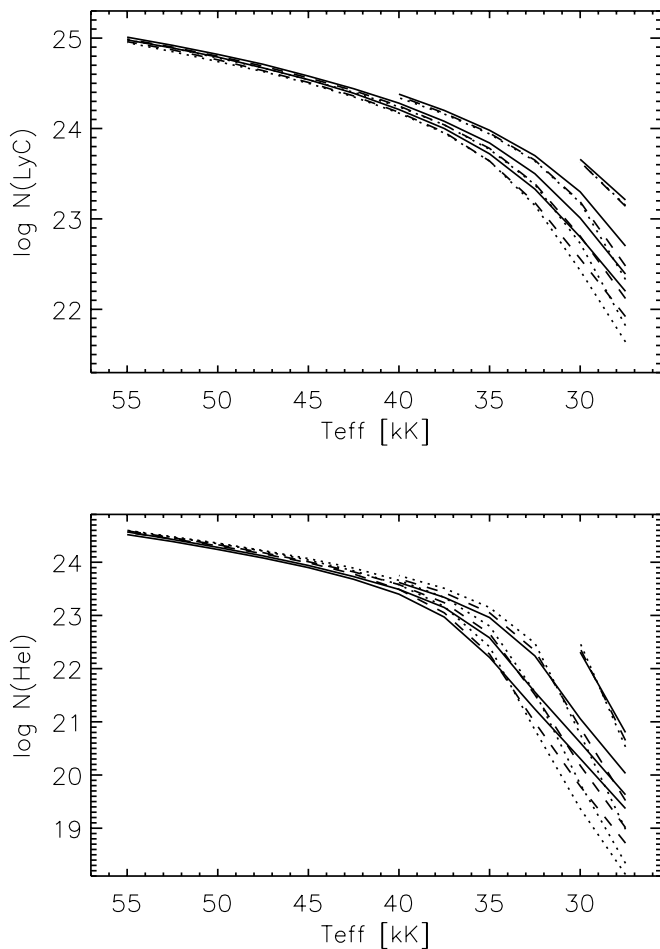
Fig. 15.—Ionization fluxes (s^{-1} cm^{-2}) vs. effective temperature. *Top:* log of number of Lyman continuum photons. *Bottom:* log of number of He I $\lambda504$ photons. In each panel, there are four families of curves from bottom to top with decreasing gravities, $\log g = 4.5$, 4.0, 3.5, and 3.0. Results for different chemical compositions are shown with different types of lines: solar (*solid line*), 1/10 solar (*dashed line*), and metal-free (*dotted line*).

1. A crude and approximate treatment of collision rates for forbidden transitions of Fe and Ni. As discussed in § 4, since no approximate formula or simple prescription is available, we have somewhat arbitrarily adopted the Eissner-Seaton formula with $\gamma(T) = 0.05$. The IRON project provides, and will keep providing in the future, theoretical calculations for selected transitions for various ions of iron; we plan to implement all the newly available collision rates in future calculations in order to check their influence explicitly.

2. A neglect of very high energy levels of light metals. The OP, which is the basic source of our atomic data, typically considers energy levels only up to a certain principal quantum number (usually 10). The higher levels are neglected. This does not usually cause any significant errors in the excitation balance, but in some cases recombinations to these neglected levels may represent a nonnegligible contribution to the total recombination rate: the global ionization balance may thus be somewhat in error.

3. Inaccuracies in, or a lack of, computed photoionization cross sections. Although the OP provided a large number of cross sections, many are still missing. We have approximated all cross sections for which we did not find

any published data by hydrogenic cross sections. However, since we have adopted accurate data for the most important transitions, we do not believe that this may be a source of significant errors.

4. We did not consider charge exchange reactions. In this case, some necessary atomic data are available, but in view of the high temperature of the atmospheres of O-type stars, we do not expect the charge exchange reactions to have any significant contribution to the computed NLTE excitation/ionization balance.

For completeness, we repeat the list of the most important physical approximations of our model grid:

1. Plane-parallel atmosphere in hydrostatic equilibrium. This is perhaps the most important and restrictive assumption. Because of its importance, we have discussed it at length in § 2.1. Essentially, we argued that while the wind features cannot obviously be described by means of our models, the rest of the UV and optical spectra are well described, unless the wind is truly extreme. In any case, the OSTAR2002 grid should not be used for analyzing luminous blue variables or Wolf-Rayet stars, where already the continuum is formed in the wind, and the grid should be used with caution in the case of Of supergiants.

2. Homogeneity (i.e., a one-dimensional atmosphere). This means that any surface inhomogeneities are neglected. However, our understanding of inhomogeneities in hot star atmospheres is very poor, and at present there is little that can be done on a quantitative level.

3. Radiative equilibrium. Our approach neglects any source of mechanical energy dissipation, shocks, nonthermal X-rays, and related phenomena. Again, there is no approach at present that would address those issues from the first principles; therefore, any modeling of such phenomena is necessarily extremely crude.

Despite the long list of approximations and uncertainties, we believe that the OSTAR2002 grid represents a definite improvement over previous grids of O star model atmospheres. We believe that we have constructed a more or less definitive grid of models in the context of one-dimensional, plane-parallel, homogeneous geometry in a hydrostatic and radiative equilibrium, with all important opacity sources (metal lines) included, and without any unnecessary numerical approximations. We hope that the OSTAR2002 grid of models will be useful for a number of years to come, until a new generation of models with multidimensional, self-consistent radiation magnetohydrodynamic description will be developed.
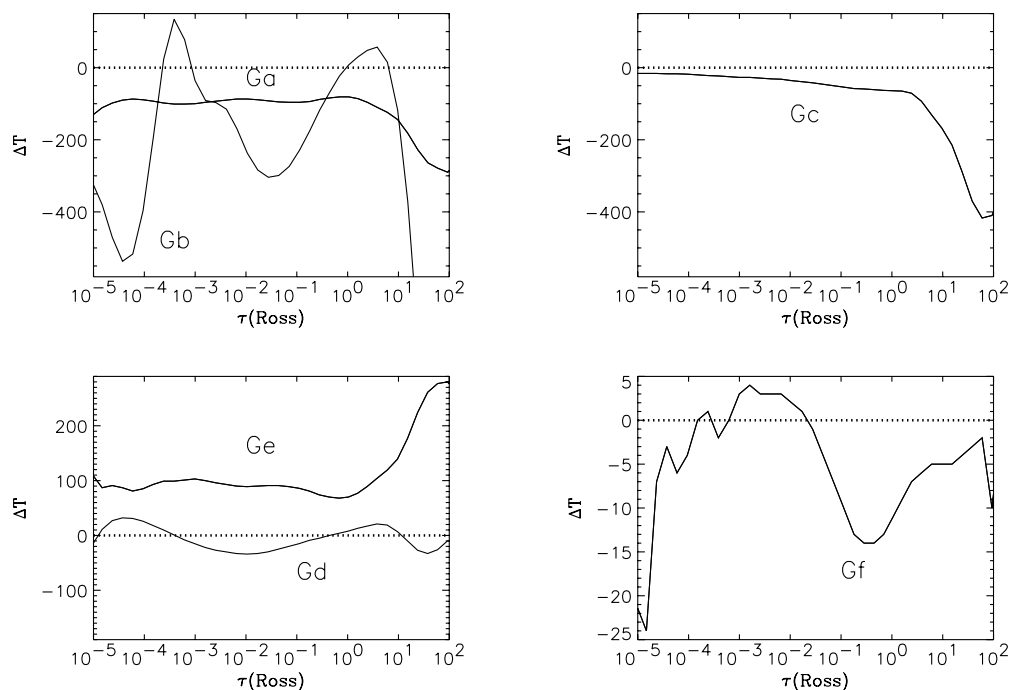
Fig. 16.—Changes in the model temperature structure with respect to the reference model depending on the treatment of Fe model atoms and line opacity (see Table 6 for model keys).

REFERENCES

Anderson, L. S. 1985, ApJ, 298, 848
———. 1989, ApJ, 339, 558
Auer, L. H., & Mihalas, D. 1969a, ApJ, 156, 681
———. 1969b, ApJ, 158, 641
Bautista, M. A. 1996, A&AS, 119, 105
Bautista, M. A., & Pradhan, A. K. 1997, A&AS, 126, 365
Bautista, M. A., Romano, P., & Pradhan, A. K. 1998, ApJS, 118, 259
Berrington, K. A., & Kingston, A. E. 1987, J. Phys. B, 20, 6631
Bessel, M. S., Castelli, F., & Plez, B. 1998, A&A, 333, 231
Bouret, J.-C., et al. 2003, ApJ, submitted
Brandt, J. C., et al. 1998, AJ, 116, 941
Butler, K., Mendoza, C., & Zeippen, C. J. 1993, J. Phys. B, 26, 4409
Charbonnel, C., Meynet, G., Maeder, A., Schaller, G., & Schaerer, D. 1993, A&AS, 101, 415
Crivellari, L., Hubeny, I., & Hummer, D. G., eds. 1991, Stellar Atmospheres: Beyond Classical Models (NATO ASI Ser. C; Dordrecht: Kluwer)
Cunto, W., Mendoza, C., Ochsenbein, F., & Zeippen, C. J. 1993, A&A, 275, L5
Deetjen, J. L., Dreizler, S., Rauch, T., & Werner, K. 1999, A&A, 348, 940
Dreizler, S., & Werner, K. 1993, A&A, 278, 199
Fernley, J. A., Hibbert, A., Kingston, A. E., & Seaton, M. J. 1999, J. Phys. B, 32, 5507
Gabler, R., Kudritzki, R.-P., & Mendez, R. H. 1991, A&A, 245, 587
Garmany, C. D., ed. 1989, ASP Conf. Ser. 7, Properties of Hot, Luminous Stars (San Francisco: ASP)
Grevesse, N., & Sauval, A. 1998, Space Sci. Rev., 85, 161
Hamann, W.-R. 1985, A&A, 148, 364
Hauschildt, P. H., Baron, E., & Allard, F. 1997, ApJ, 483, 390
Heber, U., & Jeffery, C. S., eds. 1992, The Atmospheres of Early-Type Stars (Lecture Notes in Physics 401; Berlin: Springer)
Hillier, D. J. 2003, in ASP Conf. Ser. 288, Stellar Atmosphere Modeling, ed. I. Hubeny, D. Mihales, & K. Werner (San Francisco: ASP), 199
Hillier, D. J., & Lanz, T. 2001, in ASP Conf. Ser. 247, Spectroscopic Challenges of Photoionized Plasmas, ed. G. Ferland & D. W. Savin (San Francisco: ASP), 343
Hillier, D. J., & Miller, D. L. 1998, ApJ, 496, 407
Hoeflich, P. 1995, ApJ, 443, 89

Hoeflich, P. 2003, in ASP Conf. Ser. 288, Stellar Atmosphere Modeling, ed. I. Hubeny, D. Mihales, & K. Werner (San Francisco: ASP), 185
Hubeny, I. 1988, Comput. Phys. Commun., 52, 103
———. 2003, in ASP Conf. Ser. 288, Stellar Atmosphere Modeling, ed. I. Hubeny, D. Mihales, & K. Werner (San Francisco: ASP), 17
Hubeny, I., Heap, S. R., & Lanz, T. 1998, in ASP Conf. Ser. 131, Boulder-Munich II: Properties of Hot, Luminous Stars, ed. I. Howarth (San Francisco: ASP), 108
Hubeny, I., Hummer, D. G., & Lanz, T. 1994, A&A, 282, 151
Hubeny, I., & Lanz, T. 1992, A&A, 262, 501
———. 1995, ApJ, 439, 875
———. 2003, in ASP Conf. Ser. 288, Stellar Atmosphere Modeling, ed. I. Hubeny, D. Mihales, & K. Werner (San Francisco: ASP), 51
Hubeny, I., Mihalas, D., & Werner, K., eds. 2003, ASP Conf. Ser. 288, Stellar Atmosphere Modeling (San Francisco: ASP)
Hummer, D. G., Berrington, K. A., Eissner, W., Pradhan, A. K., Saraph, H. E., & Tully, J. A. 1993, A&A, 279, 298
Hummer, D. G., & Mihalas, D. 1988, ApJ, 331, 794
Iglesias, C. A., & Rogers, F. J. 1991, ApJ, 371, 408
———. 1996, ApJ, 464, 943
Koesterke, L., Hamann, W.-R., & Graefener, G. 2002, A&A, 384, 562
Kudritzki, R.-P. 2000, BAAS, 197, 68.02
Kurucz, R. L. 1979, ApJS, 40, 1
———. 1993, Kurucz CD-ROM 13, ATLAS 9 Stellar Atmosphere Programs and 2 km/s Grid (Cambridge: SAO)
———. 1994, Kurucz CD-ROM 22, Atomic Data for Fe and Ni (Cambridge: SAO)
Lanz, T., & Hubeny, I. 2001, in ASP Conf. Ser. 247, Spectroscopic Challenges of Photoionized Plasmas, ed. G. Ferland & D. W. Savin (San Francisco: ASP), 351
———. 2003, in ASP Conf. Ser. 288, Stellar Atmosphere Modeling, ed. I. Hubeny, D. Mihales, & K. Werner (San Francisco: ASP), 117
Lanz, T., Hubeny, I., & Heap, S. R. 2003, in IAU Symp. 210, Modelling of Stellar Atmospheres, ed. N. Piskunov et al. (Dordrecht: Kluwer), in press
Luo, D., & Pradhan, A. K. 1989, J. Phys. B, 22, 3377
Martin, W. C., Sugar, J., Musgrove, A., Wiese, W. L., & Fuhr, J. R. 1999, NIST Atomic Spectra Database

Mendoza, C., Eissner, W., Le Dourneuf, M., & Zeippen, C. J. 1995, J. Phys. B, 28, 3485

Mihalas, D. 1972, Tech. Note NCAR-TN/STR-76 (Boulder: NCAR)

———. 1978, Stellar Atmospheres (2d ed.; San Francisco: Freeman)

Mihalas, D., Heasley, J. N., & Auer, L. H. 1975, NCAR-TN/STR-104 (Boulder: NCAR)

Mihalas, D., & Hummer, D. G. 1973, ApJ, 179, 827

Nahar, S. N. 1996, Phys. Rev. A, 53, 1545

———. 2003, in ASP Conf. Ser. 288, Stellar Atmosphere Modeling, ed. I. Hubeny, D. Mihales, & K. Werner (San Francisco: ASP), 651

Nahar, S. N., & Pradhan, A. K. 1993, J. Phys. B, 26, 1109

Opacity Project Team 1995, The Opacity Project, Vol. 1 (Bristol: Inst. Physics Publ.)

———. 1997, The Opacity Project, Vol. 2 (Bristol: Inst. Physics Publ.)

Pauldrach, A. W. A., Hoffmann, T. L., & Lennon, M. 2001, A&A, 375, 161

Peach, G., Saraph, H. E., & Seaton, M. J. 1988, J. Phys. B, 21, 3669

Pradhan, A. K., Zhang, H. L., Nahar, S. N., Romano, P., & Bautista, M. A. 1996, BAAS, 189, 72.11

Schaller, G., Schaerer, D., Meynet, G., & Maeder, A. 1992, A&AS, 96, 269

Seaton, M. J. 1962, in Atomic and Molecular Processes, ed. D. Bates (New York: Academic Press), 374

———. 1987, J. Phys. B, 20, 6363

Tully, J. A., Seaton, M. J., & Berrington, K. A. 1990, J. Phys. B, 23, 3811

Vacca, W. D., Garmany, C. D., & Shull, J. M. 1996, ApJ, 460, 914

van Regemorter, H. 1962, ApJ, 136, 906

Weiss, A., Abel, T. G., & Hill, V. 2000, The First Stars (Proc. MPA/ESO Workshop; Berlin: Springer)

Werner, K. 1986, A&A, 161, 177